CHEMICAL REVIEWS

Review

pubs.acs.org/CR

Structure, Function, and Mechanism of the Nickel Metalloenzymes, CO Dehydrogenase, and Acetyl-CoA Synthase

Mehmet Can,[†] Fraser A. Armstrong,[‡] and Stephen W. Ragsdale*,[†]

[†]Department of Biological Chemistry, University of Michigan, Ann Arbor, Michigan 48109, United States

[‡]Inorganic Chemistry Laboratory, University of Oxford Oxford, OX1 3QR, United Kingdom

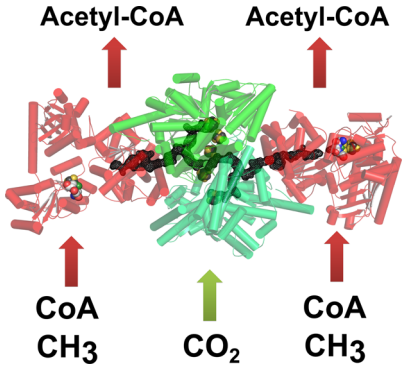

CONTENTS

1. INTRODUCTION

1.1. Research on Catalytic Reactions Involving CO and CO_2: Relationship to Energy, the Environment, Biogeochemistry, Toxicology, Health, and Technology

The major environmental- and energy-related problems facing our planet directly relate to carbon dioxide and the carbon biogeochemical cycle, which includes the biological fixation of CO_2 into organic carbon and the oxidation of fixed carbon back to CO_2. Thus, the ultimate source of all fossil fuels is CO_2, which has been fixed into organic carbon and deposited in the earth's crust over the last 4 billion years. Because modern life is so reliant on energy, particularly on fossil fuels, there is intense competition for these nonrenewable resources, thus creating a problem that has significant economic and political impacts.[1] A related problem of growing concern is the rising level of greenhouse gases, especially CO_2 and methane.

In nature, fixation of CO_2 occurs on a huge scale, with photosynthetic CO_2 fixation occurring at a rate of 200 gigatons per year.[2] There are six known pathways by which CO_2 is fixed,[3] with the Calvin cycle and photosynthesis providing most of this fixed carbon. Under anaerobic conditions, the Wood−Ljungdahl pathway is a predominant CO_2 sink, and CO dehydrogenase (CODH) and acetyl-CoA synthase (ACS), the subjects of this review, are the key enzymes in this pathway.[4]

The oxidation of organic carbon to CO_2 slightly outpaces CO_2 fixation, leaving a balance in the atmosphere. In May 2013 at Mauna Loa Observatory, the atmospheric CO_2 levels reached 400 ppm—their highest value since records began—and the levels are increasing at a rate exceeding 2 ppm per year.[5]

Special Issue: 2014 Bioinorganic Enzymology

Received: August 21, 2013
Published: February 13, 2014

   dx.doi.org/10.1021/cr400461p | Chem. Rev. 2014, 114, 4149−4174

Further increases are predicted to produce large and uncontrollable impacts on the world climate, and evidence suggests that these changes are underway.[5,6] Thus, it is important to develop renewable nonfossil energy supplies that are CO_2-neutral and easily stored, distributed, and used. CODH/ACS and the Wood–Ljungdahl pathway of CO and CO_2 fixation could play a role in this development.

Our ability to deal with these environmental- and energy-related problems will depend upon our understanding of the biology related to the global carbon cycle, especially those processes that lead to and limit CO_2 fixation. One might imagine biotechnological solutions to both the greenhouse gas and energy-limitation problems. For example, supplying limiting nutrients, e.g., iron fertilization in the Ironex experiments, can stimulate CO_2 fixation in the ocean.[7] Similarly, given the high efficiency and rates of enzymatic CO_2 activation and fixation, principles borrowed from nature are being explored to design better CO_2-reactive catalysts.[8]

While CO_2 is a relatively inert and nontoxic product of the complete oxidation of carbon, CO is a reactive, toxic gas that is produced naturally in some anaerobic bacteria by the two-electron reduction of CO_2 and in aerobic organisms by heme oxygenase-catalyzed decomposition of porphyrins.[9] CO also is generated anthropogenically by the incomplete combustion of organic materials, predominantly by the oxidation of methane and other hydrocarbons.

In the United States, poisoning by CO is responsible for ~1000 accidental deaths,[10] while more than 50 000 people per year seek medical attention for CO poisoning.[11] Faulty furnaces, inadequately ventilated heating sources, and engine exhaust exposure are the main culprits of CO poisoning. The mode of toxicity appears to be inhibition by binding tightly to the metallocenters in heme proteins, such as hemoglobin, myoglobin, and cytochrome oxidase.[12] CO emissions lead to atmospheric levels of CO ranging from 0.05 ppm in rural areas to as high as 350 ppm in some urban settings.[13] Though this level is below the toxicity threshold, the OSHA limit for CO is 50 ppm continuous exposure for 8 h. Mild effects of CO poisoning are observed in humans when CO levels remain as high as 200 ppm for 2–3 h and exposure to 1000 ppm for 1 h is fatal. Though it may seem counterintuitive, given its reputation as "silent killer" and environmental pollutant, CO, at low levels, is cytoprotective and therapeutic applications for cardiovascular diseases, inflammatory disorders, and organ transplantation are being explored.[14] This strategy follows the recognition that heme oxygenase-1 is induced during tissue injury and oxidative stress.[15]

Diverse microbes can grow on CO as their sole source of carbon and electron-equivalents.[16] This includes anaerobes such as *Moorella thermoacetica*,[17] some purple sulfur bacteria akin to *Rhodospirillum rubrum*,[18] and *Carboxydothermus hydrogenoformans*,[19] as well as some aerobic carboxydobacteria like *Oligotropha carboxidovorans*.[20] These are the organisms in which CO metabolism has been most thoroughly studied. As indicated by its low half-cell potential (−0.52 V, below), CO is a potent electron donor—approximately 1000-fold stronger than NADH—and life forms have probably utilized that property of CO as an energy source ever since life emerged 4 billion years ago in the archaean eon. Approximately 1 century ago, Haldane[21] and Leduc[22] suggested that the earliest organisms were likely to have been anaerobic autotrophs, and it has been proposed that life emerged within anaerobic hydrothermal vents by exploiting CO as a carbon and energy source.[23] The early atmosphere, which was formed by outgassing from the earth's interior by volcanoes and hydrothermal vents, is expected to have a similar composition to that of modern volcanoes and vents, with little to no O_2 and relatively high concentrations of CO_2, CO and CH_4. Hydrothermal vents, which contain dissolved CO at about 100 nM concentrations,[24] still support diverse populations of anaerobic CO oxidizers.[16,25] It has been suggested that a version of the Wood–Ljungdahl pathway may have been the first metabolic sequence to emerge, with early organisms metabolizing CO and CO_2 using ancestral forms of CODH/ACS.[3,26] Contemporary bacteria that use this pathway, such as *M. thermoacetica* and *C. hydrogenoformans*, have been proposed as models for these early chemolithotrophs.[19]

Anthropogenic CO production amounts to about 2 billion tons per year,[27] while microbial CO metabolism is partly responsible for maintaining the ambient CO below toxic levels by removing an approximately equal amount of CO from the Earth's atmosphere.[28] As described in more detail below, the microbial enzymes responsible for CO oxidation can operate at rates as high as 40 000 (mol CO)(mol enzyme)$^{-1}$ s^{-1} and catalytic efficiencies reaching 2×10^9 M^{-1} s^{-1}.[29] Anaerobic microbes can grow on CO by use of CODH/ACS, the topic of this review, to initiate metabolism by the Wood–Ljungdahl pathway, while aerobes use a Cu Mo-pyranopterin CODH that is coupled to the Calvin–Benson pathway.[30]

CO is also of great importance in the chemical industry and its reactivity is linked to formation of metal–CO bonds. For example, the M–CO complex plays a key role in industrial organometallic catalysis reactions, including the Monsanto process for acetate synthesis; the industrial Reppe process leading to the carbonylation of alkenes, alkynes, and conjugated dienes; Fischer–Tropsch reaction; hydroformylation; homologation; the water–gas shift (WGS); and hydrogenation using water as the hydrogen source.[8,31] Furthermore, we feel it is likely that interdisciplinary research on the enzymology of CO oxidation will lead to the development of novel catalysts that follow principles used by the natural catalysts for carbonylation (ACS) and reversible CO_2 reduction (CODH).

1.2. CO and CO_2 Chemistry

Carbon dioxide is the final product of the compete oxidation of carbon. A comprehensive review on CO_2 activation and reduction is available;[8] thus, we will summarize only those aspects of CO and CO_2 reactivity that are most relevant for the present review on CODH/ACS. CO_2 is very abundant in the atmosphere and stored as various forms of carbonate, yet it is relatively inert, which raises the stakes for researchers to describe strategies to convert CO_2 to useful products.

This review focuses on a two-enzyme complex that couples two extremely important reactions in biology and industry. CODH catalyzes CO_2 reduction to CO and ACS catalyzes C–C bond formation using CODH-generated CO and a methyl group to generate the key metabolic intermediate acetyl-CoA. This coupled reaction is a highly efficient biochemical equivalent of coupling the WGS reaction to the Monsanto process in a single reaction mixture. Here we will briefly review the chemical principles related to the activation and reduction of CO_2 and to the use of CO in carbonylation and C–C bond-forming reactions.

dx.doi.org/10.1021/cr400461p | *Chem. Rev.* 2014, 114, 4149–4174

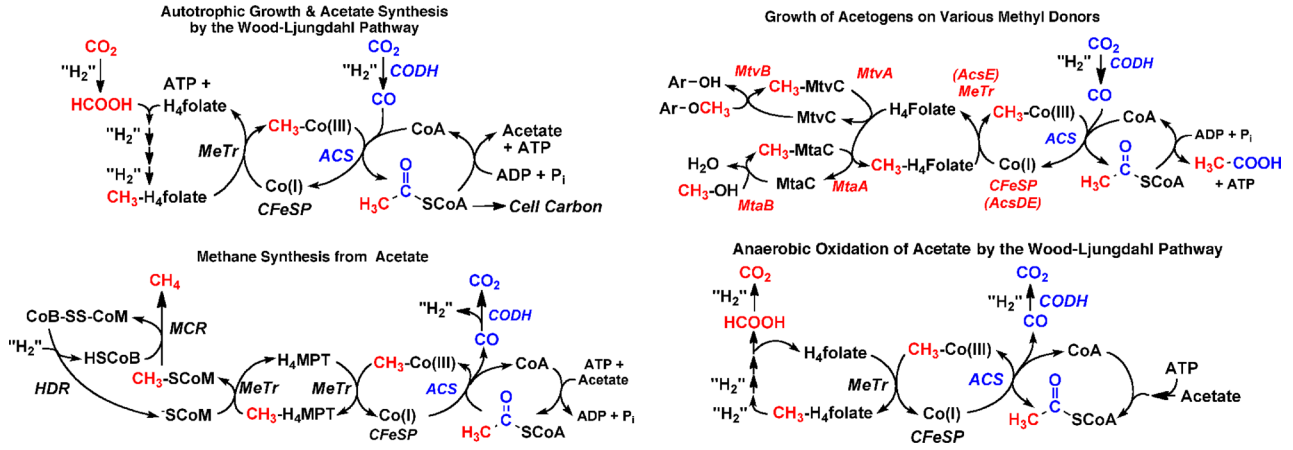

Figure 1. The Wood–Ljungdahl pathway of CO/CO_2 fixation and its involvement in acetogenesis and methyltrophy, as well as in the oxidation of acetate to methane. The methanogenic CODH/ACS is often called ACDS, acetyl-CoA synthase decarbonylase.

1.3. Introduction to CODH- and ACS-Dependent Microbial CO and CO_2 Fixation

The use of CO, a toxic gas to animals, as a metabolic building block is an interesting property of certain classes of diverse organisms that can fix CO_2 and are capable of converting CO into CO_2. CODH reversibly oxidizes CO to CO_2. This activity allows organisms to grow on CO as a sole source of carbon and energy. The CO_2 is then fixed into cellular carbon by one of the six known reductive CO_2 fixation pathways.[3] A review is available that covers the history of microbial CO oxidation and our understanding of the catalytic mechanism of CODH and ACS up until ~2003.[30]

Aerobic CO metabolism is performed by carboxydotrophic bacteria, which are aerobic microbes that grow on CO as their sole source of carbon and energy,[16] fixing CO according to eq 1.[32] Aerobic CO oxidizing bacteria are taxonomically diverse, including α-, β-, and γ-proteobacteria; Firmicutes; and Actinobacteria, including pathogenic and nonpathogenic mycobacteria.[16,33] These microbes transfer the electrons derived from CODH-catalyzed CO oxidation to O_2 through an electron transport chain involving quinones.[34] The CO_2 is assimilated into cell carbon through the Calvin–Benson–Basham pathway.[16,35] The enzyme responsible for CO oxidation is called MoCu–CODH because it contains a binuclear Mo–Cu center in which the Cu is thiolate ligated to a molybdopterin center.[36] The CODH of *Oligotropha carboxidovorans* is the most thoroughly characterized MoCu–CODH enzyme.[36,37] This three-subunit enzyme also contains two [2Fe–2S] clusters and FAD, in common with other members of the xanthine oxidoreductase family.[36,38]

$$O_2 + 2.19CO \rightarrow 1.83CO_2 + 0.36\text{cell carbon} \quad (1)$$

The Ni–CODH plays a similar role in anaerobic microbes that the Mo–Cu enzyme plays in aerobic metabolism, allowing organisms to grow autotrophically on CO by coupling CO oxidation to CO_2 fixation. Purple sulfur bacteria like *Rhodospirillum rubrum* and *Rubrivivax gelatinosus*[18] couple CO oxidation to the Calvin–Benson–Basham cycle, while methanogenic Archaea and sulfate reducing and acetogenic bacteria use the Wood–Ljungdahl pathway.[30] The CODH from the latter organisms contains a tightly associated ACS, which is purified either as an $\alpha_2\beta_2$ complex containing a central core of two CODH subunits that are associated on either side by two ACS subunits[39] or as a larger complex containing other components of the Wood–Ljungdahl pathway (e.g., the corrinoid iron–sulfur protein and methyltransferase).[40]

The association of CODH with ACS confers the ability to utilize the Wood–Ljungdahl pathway to perform diverse reactions in the carbon cycle (Figure 1). As shown in the top left panel, CODH/ACS allows organisms to grow autotrophically on CO and CO_2. In this pathway, CODH catalyzes CO_2 reduction into CO; then, ACS catalyzes the condensation of in situ generated CO with CoA and a methyl group bound to the cobalt center in a B_{12}-containing protein, to generate the key metabolite, acetyl-CoA. This mode of autotrophic growth is used by a variety of anaerobic microbes, including acetogenic bacteria and methanogenic Archaea. The Wood–Ljungdahl pathway is found in a wide distribution of phylogenetic classes, including Clostridia, Deltaproteobacteria, Chloroflexi, and Spirochaetes, and is also found in two domains (Archaea and Bacteria); however, it is found in only a few species within these classes, suggesting that this pathway was distributed by horizontal gene transfer of the core genes (CODH, ACS, MeTr, CFeSP).[41] The marker genes for the Wood–Ljungdahl pathway are *acsB* (ACS) and the two subunits of the CFeSP (*acsC* and *acsD*); as the only genes that co-occur and are co-omitted among the sequenced bacterial genomes,[41] these enzymes are undoubtedly crucial for acetogenesis.

In acetogenic bacteria, this pathway generates acetate (eq 2), conserving energy through electron transfer-linked phosphorylation. As shown in the bottom left panel (Figure 1), coupling methanogenesis to this pathway (operating in reverse) gives organisms the ability to convert acetate to methane. Sulfate-reducing bacteria can utilize the eight electrons generated during acetate oxidation (again using this pathway in reverse, bottom right scheme) to reduce sulfate to H_2S. The pathway also allows organisms to grow on various methyl donors, such as methanol and aromatic methyl ethers (top right panel). Furthermore, any oxidative pathway that generates CO_2 can potentially couple to the Wood–Ljungdahl pathway. For example, heterotrophic growth on sugars allows organisms to stoichiometrically convert glucose into 3 mol of acetate by capturing the reducing equivalents and the 2 mol of CO_2 generated by glycolytic oxidation of pyruvate to acetyl-CoA and generating a third mole of acetyl-CoA.

$$2CO_2(g) + 8H^+ + 8e^- \rightarrow CH_3COOH(aq) + H_2O$$
$$E^\circ = -0.29\ \text{V} \quad (2)$$

dx.doi.org/10.1021/cr400461p | *Chem. Rev.* 2014, 114, 4149–4174

42

2. CO DEHYDROGENASE

2.1. Redox Chemistry and Enzymology Involving CO and CO_2

Because there is such a large reservoir of CO_2 and its potential for conversion into useful products, there is much interest in the activation and reduction of CO_2. The energetic requirements for CO_2 reduction (eqs 3−8) at pH 7 vs NHE depend on the number of electrons in the redox half-reactions, as shown in eq 3−8.

$$CO_2(aq) + e^- \rightarrow CO_2^{-\bullet}(aq) \quad E^\circ = -1.9\ V \tag{3}$$

$$CO_2(g) + 2H^+ + 2e^- \rightarrow CO(g) + H_2O \quad E^\circ = -0.52\ V \tag{4}$$

$$CO_2(g) + H^+ + 2e^- \rightarrow HCO_2^-(aq) \quad E^\circ = -0.43\ V \tag{5}$$

$$CO_2(g) + 4H^+ + 4e^- \rightarrow HCHO(aq) + H_2O \quad E^\circ = -0.51\ V \tag{6}$$

$$CO_2(g) + 6H^+ + 6e^- \rightarrow CH_3OH(aq) + H_2O \quad E^\circ = -0.38\ V \tag{7}$$

$$CO_2(g) + 8H^+ + 8e^- \rightarrow CH_4(g) + 2H_2O \quad E^\circ = -0.24\ V \tag{8}$$

$$CO_2(g) + H_2 \rightarrow CO(g) + H_2O \quad \Delta E^\circ = -0.11\ V \tag{9}$$

$$2e^- + 2H^+ \rightarrow H_2(g) \quad E^\circ = -0.41\ V \tag{10}$$

The one-electron reduction of CO_2 (eq 3) requires very negative potentials, due in part to the energy required for structural rearrangement of linear CO_2 to form the bent CO_2 anion radical.[43] The high overpotential (cell potentials in excess of 2.0 V) associated with formation of this radical anion intermediate remains the major obstacle to rapid and efficient heterogeneous electrochemical reduction of CO_2.[8] On the other hand, the two-electron reduction to either CO or to formate occurs under much less demanding redox conditions (eqs 4,5). Both CO and formate formation are pH- and solvent-dependent,[44] being more favorable at low pH. The optimal catalyst for CO_2 reduction to either CO or formate should avoid the highly energetically unfavorable formation of an anion radical as a catalytic intermediate. This principle has been demonstrated with an enzyme-based CO_2 electroreduction catalyst, which rapidly generates CO via eq 4 at −0.52 V, i.e., without any overpotential.[45]

In biology, the two CO_2 reduction reactions to CO and formate are catalyzed by CO and formate dehydrogenase, respectively, which contain metal clusters to aid in CO_2 activation and electron transfer. These reactions are important in the global carbon cycle and are keys to the activation of CO_2 under anaerobic conditions.[8,46] Similarly, the synthetic catalysts that promote these reactions contain metals that bind CO_2 and facilitate electron transfer.

Homogeneous catalysts provide one mechanism for the reduction of CO_2, by hydrogenation to formate, yet to increase its reductant potential, high H_2 pressures and/or bases are used to drive the reaction.[8] The chemical interconversion between CO and CO_2 (eq 9) is an important industrial reaction called the WGS reaction, which, in the reverse direction, provides fuel-cell-grade H_2 from steam reforming.[47] In this direction, the reaction is marginally favorable with a ΔH° of −41.2 kJ mol^{-1} and a ΔG°_{298} of −28.6 kJ mol^{-1} [48] and is typically performed at temperatures greater than 200 °C using D-metal catalysts on oxide supports.[49] Because of the industrial importance, a number of laboratories in academia and industry are developing catalysts that rapidly and efficiently produce H_2 from CO and water; for example, $Ru_3(CO)_{12}$ and a recent Au−CeO_2 nanomaterial were described with a reactivity of 0.01 (mol H_2) s^{-1} (mol metal carbonyl)$^{-1}$ at 160 °C[50] and between 0.3 and 3.9 site^{-1} s^{-1} at 240 °C,[49b] respectively.

The WGS reaction is very similar to the reaction catalyzed by the enzyme CODH. In comparison, an enzyme (CODH)-based electrocatalyst yields a value for CO oxidation of >3.2 s^{-1} at 30 °C.[51] In solution, the enzymatic oxidation of CO by CODH I from *C. hydrogenoformans* ($CODH_{Ch}$ I) occurs with a turnover frequency of ∼40 000 s^{-1};[29,45a] however, in the enzymatic reaction, electrons are transferred to redox proteins (e.g., ferredoxin) that couple to other redox enzymes like hydrogenase with proton reduction being a very slow side reaction.[52] By coadsorbing the *C. hydrogenoformans* CODH and *Escherichia coli* hydrogenase to conducting graphite particles,[51] highly efficient CO-dependent H_2 production has been observed with a turnover frequency at 30 °C comparable to that of conventional high-temperature WGS catalysts (>2.5 s^{-1}) (see section 1.2).[51] This biochemical reaction performed on purified enzymes is similar to the mode by which some anaerobic microbes grow. *C. hydrogenoformans* is an anaerobic organism that can live on CO as sole carbon source, evolving H_2 as a byproduct.[29] A number of other microbes have been discovered that also adopt this seemingly extreme life style.[25,30,53]

Multielectron reduction of CO_2 is a very important reaction. Given that this process is more thermodynamically favorable than the two-electron reduction, it is somewhat surprising that such a reaction has not been discovered in nature, which instead uses discrete two-electron steps. For example, methanogenic archaea specialize in catalyzing CO_2 reduction to methane (eq 8), which, when coupled to H_2 oxidation, is thermodynamically favorable and provides energy for cellular growth.[54] Similarly, acetogenic bacteria catalyze the reduction of CO_2 to acetic acid (eq 2), coupled to the oxidation of H_2 or other electron donors. In nature, these eight-electron reduction reactions occur by discrete two-electron steps through the formate (CO), formaldehyde, methanol, and methane oxidation levels with the carbon from CO_2 bound to and transferred among organic or metallic cofactors during the process.

There are at least two reasons for the natural strategy of using enzymes that catalyze discrete two-electron-transfer steps. One is that the intermediates in the one-carbon metabolism branch off into various directions to make important cellular metabolites. Another is that the microbe is producing the final product (CH_4 or CH_3COOH) as a byproduct, with energy being conserved as ATP (through electron-transfer-linked phosphorylation) in the most thermodynamically favorable reaction(s) in the sequence.

In synthetic systems, multielectron CO_2 reduction has had limited success and the catalysts generally require large overpotentials, are unstable, and exhibit low product selectivity and yields, with the predominant industrial pathway for multielectron reduction being through CO.[8] CO is readily

dx.doi.org/10.1021/cr400461p | *Chem. Rev.* 2014, 114, 4149−4174

available as syngas (a mixture mainly of CO, CO_2, and H_2), which is produced by steam reforming (or other gasification processes) of reduced carbon-containing compounds like natural gas, coal, and biomass; however, these processes require high temperatures and are energy intensive. Thus, development of a highly efficient process for converting CO_2 to CO would have high impact on hydrocarbon production from CO_2.

Interestingly, there are no known enzymatic catalysts for multielectron CO reduction; however, nitrogenase, which functions in nature to catalyze the eight-electron reduction of N_2 and two protons to form H_2 and ammonia, providing fixed nitrogen into the global nitrogen cycle,[55] has been modified by mutagenesis to catalytically reduce CO directly, albeit very slowly.[55a,56] The related vanadium-based nitrogenase slowly reduces CO to form a variety of short chain hydrocarbons, including ethylene, ethane, propane, and propylene.[57] In the formation of hydrocarbons from CO by nitrogenase, CO binds to Fe atom(s) on one face of FeMo-cofactor.[58]

A number of chemical catalysts have been developed for multielectron reduction of CO, though most require high temperatures and pressures and produce mixtures of products.[8] For example, Fischer–Tropsch conversion of CO to methanol and other hydrocarbons using Cu/ZnO catalysts is a well-developed and efficient process.[59]

2.2. Characteristics of Ni–CODHs

2.2.1. Enzymatic Activities. Ni–CODHs can catalyze the reversible conversion of CO to CO_2 with specific activities as high as 15 756 U/mg (k_{cat} of ~39 000 s^{-1}) reported at pH 8 and 70 °C for CODH I from *C. hydrogenoformans* ($CODH_{Ch}$ I) using conventional kinetic assays.[29] Other two well-studied Ni–CODHs, CODH from *R. rubrum* ($CODH_{Rr}$) and CODH/ACS from *M. thermoaceticum* ($CODH/ACS_{Mt}$), are reported to oxidize CO at k_{cat} values of ~10 000 and ~3000 s^{-1}, respectively.[60,60b] The high catalytic rates and their wide range among different CODHs attract significant interest; however, various properties of these enzymes have made it difficult to perform mechanistic investigations and structural studies. Perhaps the most challenging issue is that the Ni–CODH is extremely oxygen-sensitive; therefore, growth of the organism and purification and manipulation of the enzyme require the strict avoidance of contact with oxygen. This is most easily accomplished by performing studies within an anaerobic chamber whenever possible and by using Schlenck line techniques for any investigations outside the chamber. For example, the glovebox within the authors' laboratory maintains the oxygen level below 2 ppm. The rapid catalytic turnover frequencies pose problems because most stopped-flow and freeze-quench instruments have dead times in the 1 ms range, while under optimal catalytic conditions, the half-time for all intermediate steps in the reaction cycle must be greater than 0.2 ms (0.7/3000) for even one of the least active enzymes (that from *M. thermoacetica*). Yet these issues have been mostly overcome by performing rapid kinetic experiments at low temperatures and/or at suboptimal pH values.[61]

CO_2 becomes a substrate for CODHs at redox potentials below ca. −300 mV, and the turnover frequency is in the range of 10 s^{-1}, which is significantly lower than the k_{cat} values for CO oxidation.[62,63] Electrochemical studies showed that $CODH/ACS_{Mt}$ catalyzes CO_2 reduction very efficiently with almost no overpotential.[64] Reduction of CO_2 to CO plays a key role in the Wood–Ljungdahl pathway[65] (Figure 1) and could allow fuel production if an efficient large-scale enzymatic electrocatalyst could be achieved. Experiments with electrode-immobilized CODH are described below in section 2.5.

Catalytic reactions reported for Ni–CODHs are not limited to CO/CO_2 conversion. $CODH_{Rr}$ produces formate as a slow side reaction during CO_2 reduction in its nickel-containing and nickel-deficient forms.[66] $CODH/ACS_{Mt}$ can convert nitrous oxide to dinitrogen in the presence of a low-potential electron donor.[67] $CODH/ACS_{Mt}$ has been shown to catalyze the anaerobic reduction of 2,4,6-trinitrotoluene, a dangerous pollutant.[68] Furthermore, $CODH/ACS_{Mt}$ can catalyze the oxidation of *n*-butyl isocyanide (*n*-BIC) to *n*-butyl isocyanate (*n*-BICt).[69] In addition, the C531A and H265 V variants of recombinant $CODH_{Rr}$ catalyze H_2 oxidation and hydroxylamine reduction, respectively.[70]

2.2.2. Structural and Spectroscopic Properties, Metal Clusters, and Redox Chemistry. The X-ray structures of five Ni–CODHs have been reported. These include structures of three bacterial (*M. thermoacetica*, *C. hydrogenoformans*, and *R. rubrum*) and one archaeal (*Methanosarcina barkeri*) enzyme.[39,71] The bacterial enzymes have sequence similarities between 46% (*C. hydrogenoformans* and *R. rubrum*) and 63% (*M. thermoacetica* and *R. rubrum*) and structures that are nearly identical (RSMD of ~0.95 Å according to PDB 1MJG and 1JQK). Crystal structures clearly reveal the presence of five metal clusters per homodimeric enzyme, two nickel–iron–sulfur clusters, called the C-clusters, one Fe_4S_4 D-cluster; and two Fe_4S_4 B-clusters, as shown in Figure 2.[39b,71b,39a,71a] The

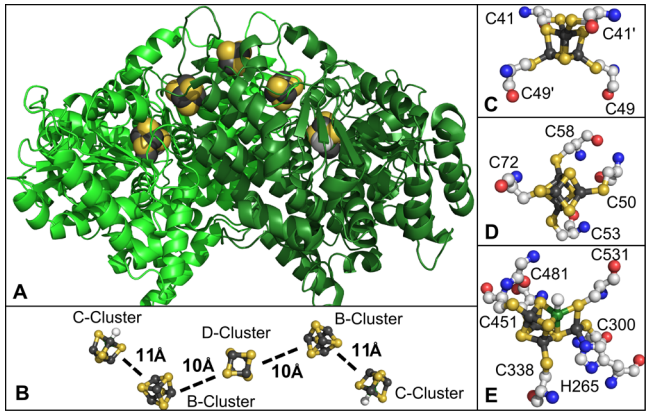

Figure 2. (A) Structure of $CODH_{Rr}$ in cartoon representation, (B) distances between the metal clusters, (C) structure of the D-cluster, (D) structure of the B-cluster, and (E) structure of the C-cluster. Atom colors: dark gray (iron), orange (sulfide), red (oxygen), blue (nitrogen), white (carbon), dark green (nickel). Generated using Pymol from PDB 1JQK.

structures also reveal why all CODHs are dimeric—there is a single D-cluster that bridges the two subunits; furthermore, the C-cluster of one subunit and the B-cluster of the other are closer than those from the same subunit. Thus, a functional dimer is required for rapid electron transfer. The methanogenic CODH contains two more Fe_4S_4 clusters (E- and F-clusters) than the bacterial enzymes. Since one subunit is positioned over the D-cluster of this enzyme, E- and F-clusters are proposed to be part of the electron transfer chain.[71i] This proposal is supported by the high sequence similarity between the FeS domain bearing E- and F-clusters and *M. barkeri* pyruvate ferredoxin oxidoreductase, electron donor for ferredoxin, and the location of these clusters between the surface and the B-

dx.doi.org/10.1021/cr400461p | *Chem. Rev.* 2014, 114, 4149–4174

Table 1. Spectroscopic and Electrochemical Data for the Ni−CODHs from Different Sources

	A-cluster		B-cluster		C-cluster	
	g-values (−CO)	E_0'	*g*-values	E_0'	*g*-values	E_0'
R. rubrum[74,89]			2.04, 1.94, 1.89	−418	2.03, 1.88, 1.71	−110
					1.97, 1.87, 1.75	
C. hydrogenoformans[88]			2.04, 1.93, 1.89		2.01, 1.89, 1.73	
					1.96, ?, 1.77	
M. thermoaceticum[79b]	2.08, 2.07, 2.03		2.04, 1.94, 1.90	−440	2.01, 1.81, 1.65	−220
	2.06, 2.05, 2.03	−530			1.97, 1.87, 1.75	−530
M. thermoaceticum with azide[90]					2.34, 2.07, 2.03	
					2.34, 2.11, 2.04	
M. barkeri[91]			2.05, 1.94, 1.90	−390	2.01, 1.91, 1.76	−35
					?, ?, 1.73	
M. soehngenii[92]			2.05, 1.93, 1.86	−410	2.01, 1.89, 1.73	−230
M. thermophila[93]	2.06, 2.05, 2.03		2.04, 1.93, 1.89	−444	2.02, 1.87, 1.72	−154
					?, ?, 1.79	

cluster. Structures of the B-, C-, and D-clusters are shown in Figure 2.

Magnetic circular dichroism (MCD), resonance Raman (rR), and electronic absorption spectroscopic studies on the nickel-deficient $CODH_{Rr}$ support the presence of two different types of $[Fe_4S_4]^{2+/+}$ clusters, presumably consisting of the bridging D-cluster and the two B-clusters.[71b,a,72] The midpoint potential of the B-clusters, between −300 and −530 mV, is consistent with an electron transfer role.[72] Interestingly, the D-cluster adopts a diamagnetic 2+ state at potentials higher than −530 mV.[72] Although the D-cluster shows an unusually low redox potential, its proximity to the surface and the B-cluster would be consistent with an electron transfer role in the CODH mechanism, though the role of this cluster has not been established.

Reversible CO/CO_2 conversion was shown to occur at the C-cluster;[61,62a,73] thus, there is much interest in characterizing this metal center, which is composed of an iron−sulfur cluster combined with a nickel atom.[74−76] Four different oxidation states for the C-cluster have been suggested: a catalytically inactive and EPR-silent C_{ox} state; a one-electron reduced C_{red1} state, which binds CO and has an electron paramagnetic resonance (EPR) spectroscopic signal with *g*-values at 2.01, 1.81, and 1.65 (g_{av} = 1.82); a two-electron-reduced EPR-silent C_{int} state;[77] and a three-electron-reduced form, C_{red2}, which binds CO_2 and has a distinct EPR signature with *g*-values of 1.97, 1.87, and 1.75 (g_{av} = 1.86).[74,78] The electronic structure of these redox states is not clear yet; however, the majority of unpaired electron spin density is localized on Fe in both C_{red1} and C_{red2}, which exhibit large ^{57}Fe and small ^{61}Ni hyperfine values.[79] The *g*-values and midpoint redox potentials for the metal clusters of CODHs from various organisms are shown in Table 1.

The nickel, iron, and sulfide content; molecular structure; and redox properties of the C-cluster have been the subject of many spectroscopic and structural studies (Figure 3).[74,75,79b,80−85] The X-ray diffraction structures and anomalous dispersion experiments revealed that Ni in the C-cluster is a part of a slightly distorted iron−sulfur cubane. Another iron atom in the C-cluster, but outside the cubane, was assigned as ferrous component II (FCII) (also called unique iron and the pendant Fe), according to a Mossbauer study.[85b] For the C_{red1} state, a ferrous component III (FCIII) was also described while other two irons were assigned to be mixed valence $Fe^{2+}Fe^{3+}$.[74] Thus, according to this scenario, C_{red1} would consist of three

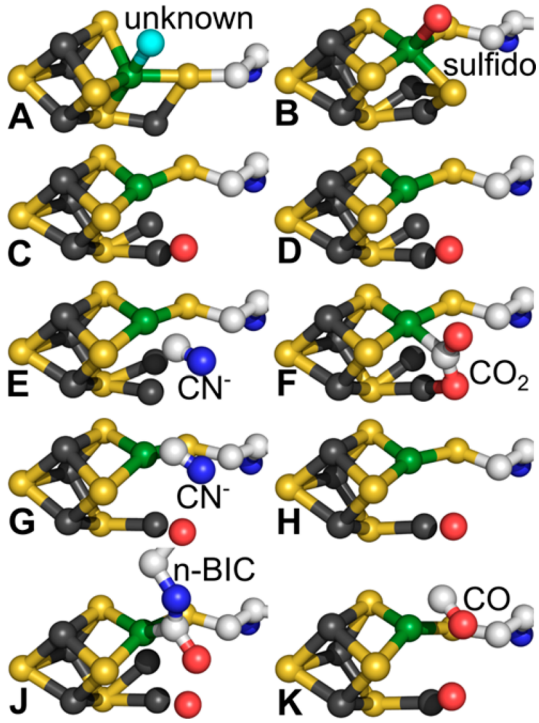

Figure 3. Structure of C-cluster including only one coordinating residue, cysteine, and the ligands from (A) $CODH_{Rr}$ (PDB 1JQK), (B) $CODH_{Ch}$ II (PDB 1SU8), (C) $CODH_{Ch}$ II at 320 mV (PDB 3B53), (D) $CODH_{Ch}$ II at 600 mV (PDB 3B51), (E) cyanide-bound $CODH_{Ch}$ II at 320 mV (PDB 3I39), (F) CO_2-bound $CODH_{Ch}$ II at 600 mV (PDB 3B52), (G) cyanide-bound $CODH/ACS_{Mt}$ (PDB 3I04), (H) $CODH/ACS_{Mt}$ (PDB 3I01), (J) *n*-BICt-bound $CODH/ACS_{Mt}$ (PDB 2YIV), (K) CO-bound $CODH_{Mb}$ (PDB 3CF4). Atom colors: Dark gray (iron), orange (sulfide), red (oxygen), blue (nitrogen), white (carbon), dark green (nickel).

ferrous and one ferric iron. The initial crystal structure of *C. hydrogenoformans* CODH II ($CODH_{Ch}$ II) included a bridging sulfido ligand connecting nickel and the pendant iron, indicating the cluster composition as $[NiFe_4S_5]$,[71b] with the bridging sulfide proposed to serve an undetermined catalytic role.[71c] However, crystal structures for $CODH_{Rr}$,[71a] $CODH/ACS_{Mt}$,[39a,b] and another $CODH_{Ch}$ II crystal structure[86] do not include the bridging sulfide. Furthermore, sulfide appears to reversibly inhibit $CODH_{Rr}$ and $CODH/ACS_{Mt}$.[87,88] Inhibition

dx.doi.org/10.1021/cr400461p | Chem. Rev. 2014, 114, 4149−4174

Table 2. Key Residues in the Primary and the Secondary Coordinating Spheres of the Metal Centers in Different Ni−CODHs

organism (PDB ID)	A-cluster	B-cluster	C-cluster	D-cluster	His-tunnel	acid−base
Rr (1JQK)		C50	C300, C338	C41, C49	H95	K568
		C53	C451, C481	C41′, C49′	H98	H95
		C58	C531, H265		H101	D223
		C72				W575
Ch (3B51)		C48	C295, C333	C39, C47	H93	K563
		C51	C446, C476	C39′, C47′	H96	H93
		C56	C526, H261		H99	D219
		C70			H102	W570
Mt (1OAO)	C506, C509	C68	C317, C355	C59, C67	H113	K587
	C518, C528	C71	C470, C500	C59′, C67′	H116	H113
	C595, C597	C76	C550, H283		H119	D241
	G596	C90			H122	W594

by sulfide and other ligands, which bind to different oxidation states of the C-cluster, will be discussed in more detail below in section 2.2.3. It is now accepted by the community that there is no bridging sulfide between Ni and the pendant Fe in the active form of the C-cluster. This Fe-bound hydroxide is viewed as the nucleophile that attacks a Ni−CO to generate a metal-bound carboxylate during the catalytic cycle.[71d,85c,94] It has been suggested that sulfide acts as a reversible inhibitor by replacing the catalytically important hydroxide.[87,88] Crystallographic studies of the carboxylate-bound state,[71a] observation of COS as a substrate,[95] and weak CO-dependent hydrogen evolution activity of CODHs[96] support this proposal. The CODH structure in its C_{red1} state reported by Jeoung and Dobbek also is interpreted to have a bridging hydroxide between Ni and pendant Fe. ENDOR spectroscopy of C_{red1} reveals the proton from the metal-bound hydroxyl group while C_{red2} appears to lack this spectral feature.[85c] On the other hand, in the C_{red2} state, a bridging hydride was proposed upon computational calculations.[97,98] Structural changes upon catalytic activity will be discussed later.

Accessory proteins (CooC, CooT, and CooJ), whose genes are part of a CODH-containing gene cluster in *R. rubrum*, appear to be required for assembly of the C-cluster.[99] Deletion of CooC, which has ATPase and GTPase activity and a nucleotide-binding P-loop region, leads to a C-cluster that contains the Fe−S but lacks Ni components of the cluster.[99,100] This Ni-deficient form of $CODH_{Rr}$ can be activated in vitro by incubation of the reduced protein with $NiCl_2$.[101] However, a similar role for AcsF, the *M. thermoacetica* homologue of CooC, could not be established.[102] On the basis of homology with HypC, CooT may be involved in metal ion discrimination.[99] CooJ has a histidine-rich C-terminus and binds up to four nickel ions per monomer.[103]

As shown in Figure 2, the C-cluster is deeply buried inside the enzyme with the C-, B-, and D-clusters aligned as an efficient redox wire with 10−11 Å intercluster distances to allow rapid electron transfer.[71b] The structures of CODH/ACS_{Mt}, $CODH_{Rr}$, and $CODH_{Ch}$ II are very similar, with strict conservation of all amino acid residues that ligate the metal clusters (Figure 2, Table 2). Other residues that are thought to be important in acid−base chemistry are also identified in Table 2.

2.2.3. Inhibition of CODH Enzymatic Activity. Several molecules including nitrous oxide, sulfide, azide, thiocyanate, cyanate, cyanide, and *n*-BIC are known to inhibit the catalytic activity of CODHs.[60b,67,69,71c,88,90,104] Here we will describe research on these inhibitors that has helped to enlighten the CODH catalytic mechanism.

Electrochemical studies combined with EPR spectroscopy showed that cyanate, an analogue of CO_2, binds the C_{red2} state and inhibits CO_2 reduction.[88] Most likely it binds to the active site in a similar fashion as CO_2 and could be used in structural studies. Inhibition of CO oxidation is limited to a very narrow potential range, with almost no inhibition occurring at potentials more positive than −0.4 V.[88] Binding of cyanate is slow, requiring several seconds with millimolar concentrations. On the other hand, isocyanides (e.g., *n*-BIC), which have been previously used as CO analogues,[36,105] can act both as a substrate and an inhibitor of CODH/ACS_{Mt}.[69,71h] Since CODH catalyzes the oxidation of *n*-BIC to *n*-BICt much more slowly (10^5-fold) than CO oxidation, *n*-BIC behaves as a rapidly binding competitive inhibitor of CO oxidation with a K_i value of 1.66 mM.[69] The crystal structure of $CODH_{Ch}$ II treated with *n*-BIC reveals the C-cluster in an *n*-BICt-bound state containing a Ni−C bond and a hydroxyl group attached to the pendant iron (Figure 3J).[71h] A hydrogen-bonding network that likely plays a role in stabilizing the C-cluster-bound CO_2 includes the iron-bound hydroxyl, a free water molecule, the oxygen of the *n*-BICt, and two residues, His93 and Lys563.

Cyanide, an analogue of CO, is a reversible inhibitor of CODH.[71f,g,82,94,104,106,107] Depending on the conditions, cyanide can act as a rapid reversible inhibitor or a slow binding inhibitor.[106a] When cyanide binds to the C-cluster in the C_{red1} state, it forms a complex with an EPR spectrum that exhibits a g_{av} of 1.72 (g = 1.55, 1.78, 1.87).[104,106a,108] CN^- does not interact with the C_{red2} state nor does it inhibit reduction of CO_2.[88] Several studies suggested the nickel as the binding site for the cyanide,[104,106a,109] while, based on the results of ENDOR[85c] and Mossbauer[74] studies, the iron was proposed as the binding site. Furthermore, it was proposed that cyanide may bind to multiple sites.[94] Furthermore, different binding modes, bent[71f] or linear,[71g] are suggested according to different crystal structures (Figure 3E,G). In the bent binding mode, there is still a water molecule bound to the pendant Fe, while there is no pendant Fe-bound water in the linear cyanide binding mode. A rearrangement is suggested to occur upon the rapid reversible binding of cyanide to yield a more stable cyanide adduct represented by the linear binding mode.[71g,94] ENDOR and Mossbauer results, previously interpreted as an evidence for cyanide binding to the pendant Fe, most likely represent a change on the water binding/leaving due to the linear binding mode of cyanide.

dx.doi.org/10.1021/cr400461p | *Chem. Rev.* 2014, 114, 4149−4174

Sulfide (S^{2-}, HS^-, or H_2S) has been proposed to act both as inhibitor[87,88] and as activator,[104,110] and its existence and role as a bridging ligand between Ni and the pendant Fe in the C-cluster have been controversial (as mentioned in the previous section). Sulfide inhibits CO oxidation, but not CO_2 reduction, as expected given that there were no significant changes in the EPR spectrum upon its addition to CODH in its C_{red2} state.[87,88,104] Furthermore, Wang et al. showed that sulfide binds the inactive C_{ox} state of the C-cluster inhibiting catalytic activity in the −50 and −250 mV potential range.[88]

2.3. Catalytic Mechanism of CO Oxidation and CO_2 Reduction

2.3.1. Metal-Based Catalysis of the Water−Gas Shift Reaction. The proposed CO/CO_2 conversion mechanism discussed here is analogous to the water−gas shift reaction described in Scheme 1.

Scheme 1. Mechanism of the Water−Gas Shift Reaction

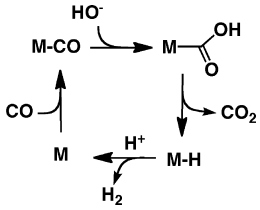

In both reaction mechanisms, CO and hydroxide ion are bound to two different metal centers that should be positioned in a proper geometry during the catalysis to allow the hydroxide to attack the M−CO intermediate, resulting in the formation of M−COOH. Release of the CO_2 from the metal complex is coupled to a hydride shift, leaving a metal hydride that undergoes protonation to generate H_2.

2.3.2. Enzymatic Mechanism of CODH. Besides the metal binding and positioning effects of the WGS catalysts, CODH is able to increase the reaction rate by optimizing the ligand binding geometry, controlling the acid−base reactions in and around the active site, enhancing substrate and product transport, and using the metal clusters as a wire to achieve a very fast electron transfer to the corresponding electron acceptors.[71b,111] In the description below, all residue numbers refer to the $CODH_{Ch}$ II. Oxidation of CO in the C-cluster occurs by a ping-pong reaction as shown in Scheme 2. In the first half reaction, the C_{red1} state of the C-cluster binds and undergoes reduction by CO and then transfers electrons from the reduced C-cluster (C_{red2}) through the B- and D-clusters in the enzyme. However, we should point out that this electron transfer role for D-cluster has not been established. Furthermore, the D-cluster is not reducible at potentials as low as −530 mV, indicating that it may serve a structural, instead of an electron-transfer role.[72] In the second half-reaction, electrons are transferred to the external redox partners, e.g., ferredoxin. The midpoint reduction potential of the C_{ox}/C_{red1} redox couple is −200 mV, while it was reported as −530 mV for the C_{red1}/C_{red2} redox couple. C_{red1}/C_{red2} redox couple reduction potential matches well for the CO/CO_2 redox potential.

Similar to the water−gas shift reaction, the first catalytic step is the binding of CO and water to the metal centers (Scheme 2). On the basis of the results of ENDOR spectroscopic[85c] and X-ray crystallographic[71a,b] studies, the catalytic water (hydroxide) molecule binds to the pendant Fe site of the C-cluster and also associates through H-bonding interactions with Lys563, His93, and His263 (Figure 4). These residues are proposed to participate in acid−base reactions, including formation of active Fe(II)−hydroxide.[71a,b] Site-directed substitutions of Lys563 and His113 abolish enzymatic activity, confirming the importance of these residues in catalysis.[112] A histidine tunnel composed of histidine residues located on sequential turns of a helix starting near the C-cluster and ending at the protein surface is proposed to facilitate transfer of protons during the reaction (Figure 4).[71a,112] Steady-state kinetic studies conducted using NMR spectroscopy support the presence of a rich proton reservoir inside the enzyme.[94]

CO binds to the C_{red1} state of the C-cluster with a diffusion-controlled rate constant greater than 2×10^8 M^{-1} s^{-1} (a value that is 10-fold faster than k_{cat}/K_m) according to rapid freeze quench EPR,[61] NMR, and steady-state kinetic studies.[94]

Scheme 2. Proposed Catalytic Mechanism of Reversible Carbon Monoxide Dehydrogenase[a]

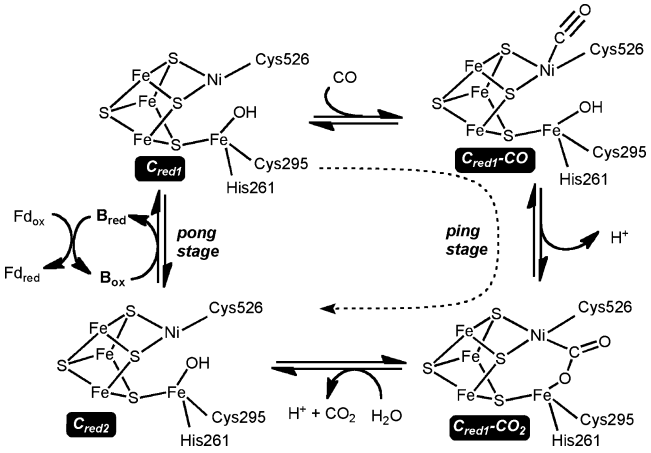

[a]The most well-characterized ferredoxin (Fd) from *M. thermoacetica* and many other organisms contains two $[Fe_4S_4]$ clusters and thus can accept two electrons. For a Fd containing a single cluster, two Fd would be required.

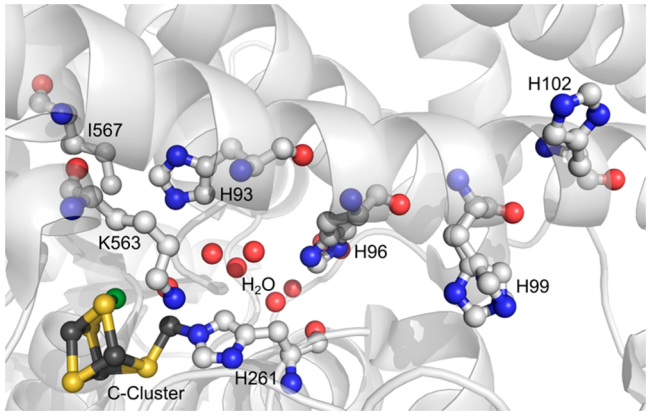

Figure 4. Structure of the C-cluster from $CODH_{Ch}$ II at 600 mV including only one coordinating residue: histidine and the ligands proposed to be important in catalytic activities. Atom colors: Dark gray (iron), orange (sulfide), red (oxygen), blue (nitrogen), white (carbon), dark green (nickel). Unbound red spheres represent the water molecules. Generated using Pymol from PDB 3B51.

dx.doi.org/10.1021/cr400461p | *Chem. Rev.* 2014, 114, 4149−4174

However, the rate of reduction of the B-cluster (3000 s^{-1})[61] is only slightly higher than the steady-state k_{cat}, indicating that this step is partially rate-limiting in the CODH mechanism. On the basis of NMR and steady-state kinetic studies, release of CO_2 has also been proposed to be partly rate-limiting.[94] Binding of CO to CODH/ACS is associated with Fourier transform infrared (FTIR) bands at 1901, 1959, 1970, 2044, and 2078 cm^{-1}, assigned to the Ni−CO stretching mode.[85a] The absence of any IR bands in this region for the as-isolated CODH/ACS_{Mt} suggests that the intrinsic Ni−CO ligand seen in hydrogenases[113] is not present in CODH. Extended X-ray absorption fine structure (EXAFS) spectroscopy reveals the presence of Ni^{2+} in the as-isolated C_{red1} state of $CODH_{Ch}$. Treatment of the enzyme with CO or Ti^{3+} changed the Ni K-edge shape slightly but does not shift the edge significantly. In both cases, the average Ni−S distance increases to 2.25 Å, making the Ni site more tetrahedral. Similarly, significant changes in the EXAFS analysis upon CO treatment suggest a structural rearrangement in the C-cluster, but without any changes in the Ni oxidation state. The only crystal structure that depicts a Ni−CO complex in a CODH is that of the CODH ($CODH_{Mb}$) portion of *M. barkeri* ACDS (Figure 3K), which, like the other CODHs, shows a water ligand bound to the pendant Fe.[71i] CO is bound to the Ni in a bent fashion, with an angle of 103°, which could contribute to the high turnover numbers by destabilizing the ground state of the Ni−CO intermediate. The crystal structure of the complex between cyanide and CODH/ACS_{Mt} reveals a similarly bent Ni−CN bond (Figure 3G),[71f] supporting a bent Ni−CO bond with the substrate. It was proposed that a conserved isoleucine residue very close to the bound-CO could sterically block the linear binding of the CO.[71f] It should be pointed out that an independent scrutiny of the crystallographic data, including a recalculation of the electron density, did not find evidence for the CO-ligand in the $CODH_{Mb}$ structure and for the CN ligand in $CODH_{Mt}$ structure.[114] In another structure of the CN complex, in this case with $CODH_{Ch}$, the Ni−CN is linear (Figure 3E). A computational study indicated that Ile567 (Figure 4) plays a steric role and that Lys563 and the histidine residues are involved in acid−base chemistry during CO oxidation.[111]

In the second step of the catalytic cycle, the Fe-bound hydroxide attacks the Ni−CO. FTIR studies support the formation of a metal carboxylate.[85a] On the basis of the crystal structure of a bicarbonate-soaked $CODH_{Ch}$ II crystal, the Ni and Fe subcomponents of the C-cluster are bridged by a carboxylate, indicating that this could be a catalytic intermediate formed by attack of the hydroxide to the Ni−CO (Figure 3F).[86] Superimposition of the C-clusters of CO-bound $CODH_{Mb}$ with CO_2-bound $CODH_{Ch}$ II suggests a significant shift in the carbon atom's position, which is proposed to change the nickel coordination from tetrahedral to square planar in the CO_2-bound form.

The third step includes the generation and release of CO_2 and a proton, and the reduction of the C-cluster from C_{red1} to the C_{red2} state, which thus should be two electrons more reduced than C_{red1}. While reduction of C_{red1} to C_{red2} upon reaction with CO is very fast (>2 × 10^8 M^{-1} s^{-1}),[61,84] release of CO_2 is proposed to be slow on the basis of NMR and steady-state kinetic studies.[94] Note that in the WGS reaction (above), this step involves a hydride migration, leaving the metal center in the same redox state. For several reasons, including the similarity of the EPR signals of C_{red1} and C_{red2}, it was proposed that a metal hydride is also formed during this part of the CODH reaction cycle.[114] A related proposal is that two-electron reduction of the C-cluster generates a Ni^0 state.[115] Because Ni(0) would be a diamagnetic species in a spin system with most of the electron density in the Fe−S cluster, formation of this low-valent Ni state would also be consistent with the minimal EPR spectral differences between the C_{red1} and C_{red2} states.

In the fourth step, the C-cluster returns to its resting C_{red1} state upon transfer of two electrons to the B- and D-clusters. The distance between the metal clusters is approximately 11 Å (Figure 2B), making it a good electron transfer route.[71b,116]

Rapid kinetic studies show that, at high (>K_m) CO concentrations, internal electron transfer (from the C-cluster to B- and D-clusters) can be rate-limiting during the first half-reaction;[84] however, the final step (the pong stage) of the mechanism appears to be rate-limiting during steady-state turnover.[61,84] Step 5 involves electron transfer to the final electron acceptor. CODH interfaces with many electron carriers that support different specific activities,[29,117] including small redox proteins (ferredoxin, flavodoxin, rubredoxin); cofactors [FAD and FMN, but not NAD(P)]; redox enzymes (couple directly to CODH), like pyruvate:ferredoxin oxidoreductase (PFOR); hydrogenase; and artificial electron acceptors, like bipyridyl (viologen) dyes and methylene blue.[52,82]

2.3.3. CO and Water Channels. Given that the CODH active site is buried deeply inside the protein and the catalysis rates are very high, there must be highly efficient routes to achieve optimal substrate and product flow. A very long hydrophobic channel starting from the surface of the protein directing above the apical coordination site of nickel in the C-cluster was proposed to be the substrate channel, while another channel starting approximately at the end of the proposed substrate channel and ending at the enzyme surface near the B- and D-clusters was also proposed to be the water channel.[71b] Although the recently published crystal structures support the presence of the channels, experimental support for these channels in monofunctional Ni−CODHs has been lacking. A recent X-ray crystallographic study of the interaction of $CODH_{Ch}$ II with the inhibitor and slow substrate *n*-BIC revealed the presence of two different channels: one similar to the substrate channel found in the CODH component of CODH/ACS and another substrate channel unique for monofunctional Ni−CODHs.[71h] This unique channel is blocked by several residues in bifunctional Ni−CODHs, most likely to avoid the escape of the substrates. Molecular dynamics and density functional theory computations have provided evidence for a dynamically formed gas channel in CODH/ACS for diffusion of CO_2 from solvent to the C-cluster.[118] Two cavities that are not apparent in the X-ray structures and are transiently created by protein fluctuations are proposed to form this channel.

2.4. Inorganic Modeling for CODH

2.4.1. Structural Models for the C-Cluster. Spectroscopic studies had initially been interpreted to exclude the possibility of Ni being within a cube.[119] Thus, the first publication of the crystal structure of CODH was surprising to the bioinorganic chemistry community, because it revealed the C-cluster to contain a $NiFe_3S_4$ cubane cluster bridged to another iron.[71a,b] This heterometallic cluster has proven to be one of the most difficult metal centers to model. Holm and co-workers successfully prepared the first [$NiFe_3S_4$] cubane model complex **2** (Scheme 3) by reacting **1** with $Ni(PPh_3)_4$.[120]

dx.doi.org/10.1021/cr400461p | *Chem. Rev.* 2014, 114, 4149−4174

Scheme 3. Schematic Views of Model Complexes Mimicking the C-Cluster

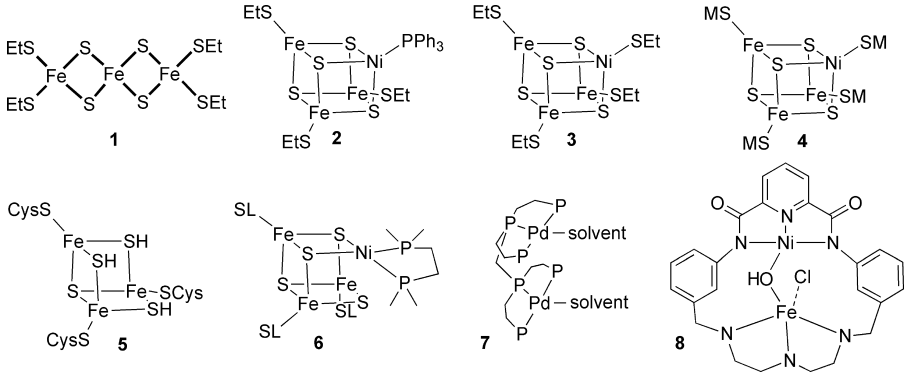

Changing the Ni ligand resulted in the synthesis of many different complexes; for example, with $Ni(SEt)_4$, **3** is obtained. Manipulation of the iron ligands by tailoring the starting linear ferric cluster **1** led to novel $NiFe_3S_4$ clusters, e.g., **4**.[121] Another modeling approach began by preparing cuboidal Fe_3S_4 clusters,[122] **5**, and incorporating different metal ions into this center, to generate a series of $[MXFe_3LS_3]$ [where LS_3 is 1,3,5-tris((4,6-dimethyl-3-mercaptophenyl)thio)-2,4,6-tris(*p*-tolythio)benzene(3−)] complexes.[123] In these model complexes, the iron atoms are bound to LS_3 ligands, making them structurally analogous to the C-cluster. Several $[NiFe_3S_4]$ complexes, including a square planar species, have been reported, e.g., **6**.[124,124b] However, among these synthetic structural models, none has yet been reported to be active in catalyzing the interconversion of CO and CO_2. Furthermore, no $NiFe_3S_4$ complex bridged to a pendant Fe like that of the C-cluster has yet been reported.

2.4.2. Functional Models for CODH. As described in a recent US Department of Energy (DOE) report,[125] "The major obstacle preventing efficient conversion of carbon dioxide into energy-bearing products is the lack of catalysts..."; thus, the development of effective catalysts for the activation, reduction, and conversion of CO_2, an abundant greenhouse gas, to fuels and chemicals would have enormous economic and environmental impact. As described in the introduction, CO_2 reduction is difficult because of both thermodynamic (the low redox potential required) and kinetic (the chemical inertness of CO_2) issues. The largest barrier that the model complexes have to overcome is the very high activation energy of the one-electron reduction of CO_2 to the radical anion (see the Introduction, the electrochemistry section below, and a recent review[8] for details). Two detailed reviews covering catalytic CODH models are available.[8,126] Thus, here we will briefly describe important conclusions from the catalytic modeling efforts and how they relate to the enzymology of CODH, as well as suggest how principles uncovered from studies of the enzyme might inform the next generation of CO_2 reduction (or CO oxidation) catalysts.

Initial efforts to accomplish CO_2 reduction included the synthesis of Co^+ and Ni^+ compounds of cyclam and its variants.[127,128] These studies showed the importance of the metal reduction potential, solvent effects, and intermolecular and intramolecular hydrogen bonding on CO_2 binding affinity and kinetics.[129,130] In the enzyme, these factors are optimized to promote proper H-bonding, salt bridge and hydrophobic interactions among residues in the overall protein structure, and appropriate geometries and distances for metals and ligands at the active site, as well as in the secondary coordination sphere.

Palladium phosphine complexes have been designed to be highly active molecular catalysts of CO_2 reduction to CO.[131−133] In these complexes, Pd^{2+} is coordinated by three phosphorus atoms, $RP(CH_2CH_2PR'_2)_2$, where R and R′ can be alkyl or aryl groups, and a solvent molecule. According to the proposed catalytic cycle,[126] the initial step includes reduction of the metal center from (2+) to (1+) oxidation state, as shown in Scheme 4. Then, in the rate determining step (at low pH

Scheme 4. Schematic View of the Proposed Intermediates in CO_2 Reduction on Palladium Catalyst

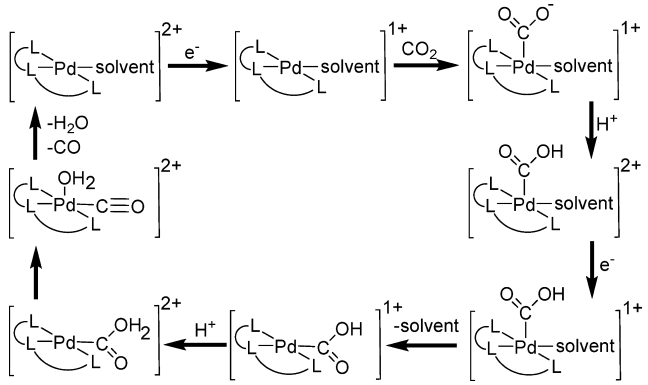

values), CO_2 binds to the Pd^+ to form a metal carboxylate at a rate that depends on the reduction potential of the metal center, with rates increasing as the potential decreases.[134] Similar initial steps are observed in Fe, Co, and Ni catalysts that require very negative potentials for one-electron reduction; however, they exhibit different rate-determining steps.[135−137] The next step is the protonation of the metal carboxylate, which promotes C−O bond cleavage and presumably is the origin of the increase in rate of CO_2 reduction as the acidity of the reaction mixture increases.[138] Then, solvent (a coordinating organic molecule, e.g., dimethylformamide) dissociates from the metal center upon another $1e^-$ reduction of the CO_2H-bound complex, leaving a vacant site on the metal.[131] Protonation of this complex forms $LPd-COOH_2$ followed by C−O bond cleavage and separation of CO and H_2O on the metal center. At low acid concentrations, the C−O bond-cleavage step becomes rate-determining.[126] In the last step, water and carbon monoxide are released from the complex and solvent coordinates again to the metal. Dissociation of the M−

dx.doi.org/10.1021/cr400461p | *Chem. Rev.* 2014, 114, 4149−4174

CO bond is very fast, since the CO affinity of Pd^{2+} is very low.[131,133]

In order to increase the CO_2 affinity of the Pd catalysts (and unwittingly generate an intermediate(s) like that observed in CODH), the bimetallic compound **7** (Scheme 4) was prepared.[139] While one Pd binds the carbon atom of CO_2, the other acts as a general base to bind the oxygen. This complex exhibits CO_2 reduction activity as high as 10^4 M^{-1} s^{-1}; however, it becomes inactivated after several turnovers, most likely due to Pd−Pd bond formation. We surmise that formation of a Ni−Fe bond would also be inhibitory to the enzymatic reaction and that this is prevented in Ni−CODHs due to the different reduction potentials of the metal centers. The general bimetallic theme is not necessarily conducive to catalysis in that compound **8**, which has a Ni−Fe bimetallic model like CODH, has no CO_2 reduction activity.[140] As a result, there is still a need to prepare and explore metallic catalysts to efficiently and economically reduce CO_2.

2.5. Electrochemical and Environmental Application Efforts

Given an abundant source of CO_2, an important aim for technology would be to achieve rapid and efficient CO_2 reduction to any of its reduction products using energy provided by electricity or solar sources. Electrochemical considerations are important in each case; a reversible electrocatalyst operates close to the reversible potential and is therefore by definition the most efficient, and efficiency is important given the cost of electricity and the need to exploit the visible region of the solar spectrum. The first 2 equiv stage of CO_2 reduction, namely, its conversion to CO or formate, formally takes us into organic chemistry, but this stage is the most demanding in terms of electrochemical potential. There are numerous efforts to find suitable catalysts for CO_2 reduction that are based on first-row transition metals; so far, the most successful electrocatalyst is Cu, although a sizable overpotential is required to drive conversions to several products. Other catalysts include polymeric Ru carbonyl complexes, compounds based on other transition elements, and even pyridinium ions, but they all fall far short of the performance observed in electrochemical studies of CODH.

Protein film electrochemistry (PFE) refers to a suite of electrochemical techniques used to study an enzyme that is attached tightly to a suitable electrode surface, usually by simple physical adsorption.[141] The electrode is rotated at various speeds in an enclosed cell containing a small volume of buffered electrolyte and connected to a gas supply that goes through the headspace and equilibrates with solution. Reagents can also be injected into the solution through a septum. Many redox enzymes have now been investigated by PFE, revealing detailed information on their catalytic activity in both oxidizing and reducing directions, as a direct function of electrode potential (E). The primary observable is the catalytic current (i), negative or positive for net reduction or net oxidation, respectively, which is directly proportional to the turnover rate at the particular electrode potential that is applied by the instrument. Specifically, the current $i_{(E)}$ observed at a particular potential is related to net turnover frequency $k_{cat(E)}$ at that particular potential by $i_{(E)} = k_{cat(E)} \cdot nFA\Gamma$, where n is the number of electrons involved (2 for CODH), F is the Faraday constant, A is the electrode area, and Γ is the electroactive coverage of enzyme. The latter is usually <1 pmol cm^{-2}, too low to observe any signals due to electrons entering or leaving the enzyme when substrate is not present to amplify the current. For a very active enzyme, the catalytic current may be large and provide an excellent handle with which to measure the extent and rates of reaction with inhibitors as these are added or removed. Use of PFE has provided new insight into why redox enzymes are so efficient, because not only does an investigator measure rates, but also the energy (strictly speaking the potential) that is required to achieve a particular rate. In principle, PFE is a new way of studying enzyme kinetics, except that the enzyme is probed using a potential in the same way as we would examine an electronic device to obtain its *iE* characteristics. Unlike potentiometry, which examines states of active sites poised at redox equilibrium, PFE examines the steady-state flow of electrons in a particular direction, and measurements may be made at any potential, often well outside the boundaries imposed by redox mediators.

The basic technique is cyclic voltammetry, in which the electrode potential is scanned linearly, back and forth, between two limits. Cyclic voltammetry, long used to characterize the reduction potentials and stabilities of small molecules in solution, has become a powerful method for studying the catalytic electron-transport properties of enzymes. Overlay of catalytic currents in each scan direction means that the catalytic activity is constantly a simple function of electrode potential; conversely, and assuming that the enzyme is stable on the electrode, hysteresis means that a change in catalytic activity occurs on a time scale that is slow compared to the scan rate. The information obtained by cyclic voltammetry provides the broader picture of what an enzyme can do over a wide potential range, paving the way for more specialized investigations, including bulk solution spectroscopic experiments designed to isolate states prevailing at a particular potential. An important electrochemical technique at this stage is controlled potential chronoamperometry, in which a reaction is initiated by a step in potential or injection of a reagent and monitored as a current−time plot; this technique is used to obtain rates of interconversions between different states of the enzyme.

An early (2007) study of $CODH_{Ch}$ I by PFE showed very easily how this enzyme operates under different mixtures of CO_2 and CO.[45a] The voltammograms in Figure 5 reveal the

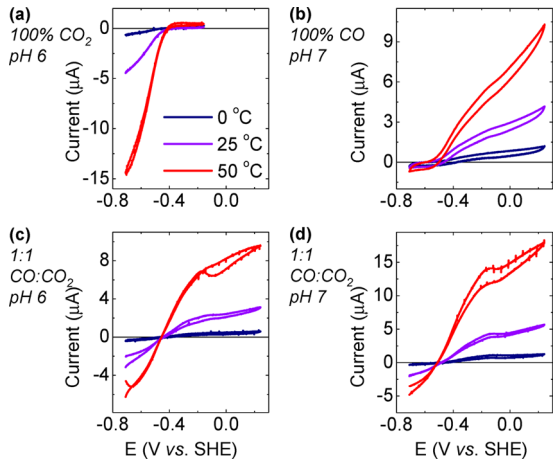

Figure 5. Protein film voltammograms showing CO_2 reduction and CO oxidation activities of $CODH_{Ch}$ I adsorbed on a PGE electrode under atmospheres of 100% CO_2, 100% CO, or 1:1 CO_2/CO gas mixtures. Scan rate was 10 mV/s in parts a, c, and d and 30 mV/s in part b. Electrode rotation 4000 rpm. Reprinted with permission from ref 45a. Copyright 2007 American Chemical Society.

dx.doi.org/10.1021/cr400461p | *Chem. Rev.* 2014, 114, 4149−4174

intense electrocatalytic activity of $CODH_{Ch}$ I adsorbed on a pyrolytic graphite "edge" (PGE) electrode rotating at high speed in an anaerobic sealed cell. Panels a and b reveal the separate reduction and oxidation activities under 100% CO_2 or 100% CO, while panels c and d show combined reduction *and* oxidation activities for a 1:1 CO_2/CO gas mixture at two different pH values. The cyclic voltammograms recorded in the presence of both CO_2 and CO immediately give us some idea of the catalytic bias of the enzyme, as explained later: they show how the current cuts cleanly through the potential axis at the values expected for the equilibrium potential of the mixture. In other words, electrocatalysis occurs close to the reversible limit with only a minuscule overpotential required to shift the reaction from one direction to the other. Temperatures are also shown and allow us immediate insight into activation energies in each direction. Such a clear example of *reversible* electrocatalysis, otherwise observed only in a few cases—notably H_2 on platinum—is emerging to be a distinctive feature of enzymes such as hydrogenases, CODH, and several other enzymes. Size, it appears, is no barrier to being the best electrocatalysts so far investigated.

The K_M values for reaction in each direction were investigated by monitoring the time course of current decrease after injecting small aliquots of solution containing CO or CO_2 into the cell, under a continuous flow of inert gas, while the rotating electrode is held at a fixed potential, i.e., −0.4 V for CO oxidation or −0.6 V for CO_2 reduction. The principle of this method is that the gas concentration decreases exponentially but a drop in current is not observed until the concentration of gas remaining approaches that of the respective K_M. At 25 °C, pH 6.0, the K_M^{CO} value (13 experiments) was estimated at ca. 0.002 atm (ca. 2 μM, using the relevant Henry's constant), but only a lower limit (ca. 0.06 atm) could be determined for $K_M^{CO_2}$. Although 25 °C is well below normal growth temperatures for *C. hydrogenoformans*, the low K_M^{CO} value reflects very well the enzyme's ability to scavenge low-level CO. The very high $K_M^{CO_2}$ value means that in Figure 5, CO oxidation activity (panel b) is saturated, whereas CO_2 reduction (panel a) is not, and at pH values below 6, extrapolated values of k_{cat} for CO_2 reduction must be higher than for CO oxidation; however, this comparison may be of academic rather than physiological interest. What is important here is that CO can be scavenged from dilute sources at potentials close to the reversible value of the CO_2/CO couple. The catalytic bias of an enzyme, in this case the efficiency with which CO is oxidized relative to the efficiency with which CO_2 is reduced, is discussed further later in this section.

Armstrong and Hirst have discussed the factors that are important for efficient electrocatalysis by enzymes.[142] The important considerations are (1) efficient long-range electron transfer (in accordance with Marcus theory, reorganization energies for electron-transfer sites are small); (2) ensuring that electrons leave or enter the catalytic cycle at a potential close to that of the redox reaction being catalyzed; (3) ideally, concerted proton−electron transfers at the active site, avoiding charge separation; and (4) the ability to provide all the electrons needed to convert reactants to products in a single stage or stabilize intermediates sufficiently to a free energy value level with that for the single multistep reaction. These factors seem to be satisfied well for CODH: first, the Fe_4S_4 clusters (D- and B-clusters) of the electron relay are optimized for low reorganization energy with potential values quite close to the CO_2/CO couple (see later); second, the active site has evolved to bind CO or CO_2 (depending on oxidation state) with little reorganization, undergo concerted proton−electron transfer, and stabilize a bound intermediate. All these properties, due to exquisite positioning of the supramolecular atomic framework around each site, appear to have been refined through evolution. Hexter and co-workers have formulated a basic model for the catalytic bias of the turnover frequency of an enzyme attached to an electrode surface.[143] This model is simplified by restricting the enzyme to have a single active form (i.e., neglecting resting states) and deals only with the limiting k_{cat} that should be obtained under substrate-saturated conditions and does not deal with substrate binding affinity. Regarding the issue of catalytic bias, the analysis based on this model asks the question "how fast can enzyme catalysis run in one direction relative to the other, when the substrate is saturating and the electrode potential in each case is set so as to provide an appropriate thermodynamic driving force?" The answer, according to the model, is that the catalytic bias to operate preferentially in one direction or the other is related to the difference between the equilibrium potential for the substrate reaction being catalyzed and the reduction potential at which electrons enter or leave the catalytic cycle, the latter being the potential-determining step and associated with a component of the enzyme termed the "electrochemical control center". For $CODH_{Ch}$ I, the electrons enter or leave the enzyme via the D-cluster, and the fact that $CODH_{Ch}$ I is a good CO_2 reducer owes much to the D-cluster having a very negative reduction potential. Further insight into the catalytic bias is provided when we consider, in addition, how tightly the different states of the enzyme bind CO or CO_2, and this aspect is discussed later.

Returning to the cyclic voltammetry of $CODH_{Ch}$ I, as the electrode potential is scanned to more oxidizing potentials, the current trace reveals hysteresis that is due to slow oxidative formation of an inactive state followed, upon the return scan, by a relatively rapid reductive reactivation. The immediate, simplistic interpretation of these results is that the oxidized inactive state C_{ox} is being formed at the electrode. From time to time, some samples of enzyme show two reactivation processes, one at a much lower potential than the other. The "sample history" dependence of the observation of a second species reactivating at a lower potential is discussed later.

The lower reductive current obtained in the presence of CO, compared to when it is absent, shows that conversion of CO_2 by $CODH_{Ch}$ I is subject to strong product inhibition.[45b] With PFE, activity measurements can be made at much more negative potentials than can easily be applied with chemical electron donors. Under more reducing conditions, i.e., below −700 mV, CO becomes much less effective as an inhibitor, as established by Lineweaver−Burk measurements of K_i as a function of potential, providing a clue that a more reduced state of the active site is unable to bind CO. Further experiments, shown in Figure 6A, showed that both oxidation of CO and reduction of CO_2 are strongly inhibited by CN^-; however, below −600 mV, the current due to CO_2 reduction increases strongly as CN^- is released from the more reduced active site that now prevails. All these observations are explained in terms of CO and isoelectronic/isostructural CN^- targeting and stabilizing the state C_{red1}. The PFE technique clearly shows that CN^- ceases to be an inhibitor when the active site is in the C_{red2} state.

Reduction of CO_2 is inhibited by cyanate (NCO^-), which is isoelectronic and isostructural with CO_2, and PFE reveals an

dx.doi.org/10.1021/cr400461p | *Chem. Rev.* 2014, 114, 4149−4174

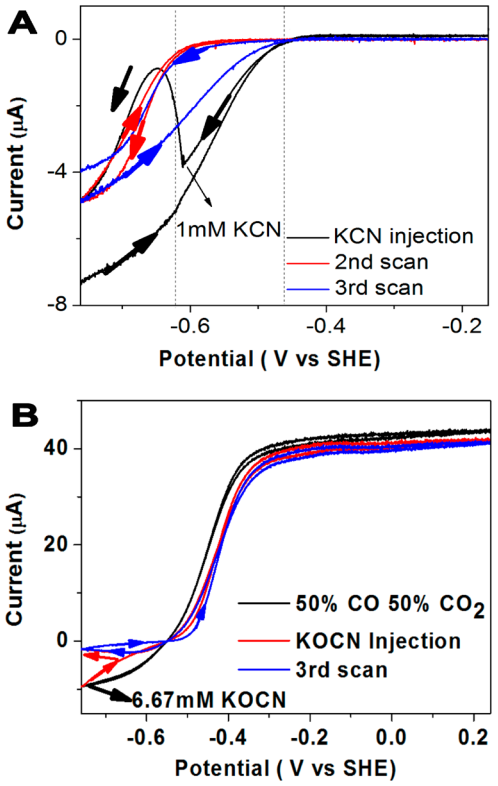

Figure 6. Voltammograms showing, for $CODH_{Ch}$ I, (A) the potential dependence of inhibition of CO_2 reduction activity upon injection of cyanide (CO oxidation is completely inhibited), pH 7.0, scan rate 1 mV s^{-1} and (B) inhibition of CO_2 reduction activity and shift in potential for CO oxidation upon addition of cyanate, pH 7.0, scan rate 1 mV s^{-1}. Adapted with permission from ref 45b. Copyright 2013 American Chemical Society.

interesting effect on CO oxidation, in that a small overpotential is required to achieve conversion (Figure 6B). The result is explained by NCO^- binding preferentially to C_{red2} and stabilizing this state, so the catalytic current commences only after the potential favors C_{red1} and causes release of the inhibitor.

The inhibitors CN^- and NCO^- are thus complementary: each targets a different redox state of the active site, as analogs of either CO or CO_2. In terms of kinetics, however, the inhibitors behave differently to the natural substrates, as binding and release of CN^- and NCO^- from the active site are orders of magnitude slower than the turnover rates observed for CO and CO_2. These slow rates could stem from requirements for protonation and deprotonation (HCN/CN^-), differences in charge (NCO^- is the conjugate base of a strong acid), and ease of rehybridization upon binding or release. The studies carried out originally with $CODH_{Ch}$ I have been repeated with $CODH_{Ch}$ II, showing that similar (but not identical behavior) is observed with the crystallographically characterized isozyme.[144] For example, CO_2 reduction by $CODH_{Ch}$ II is more strongly inhibited by CO than $CODH_{Ch}$ I, a property that may have physiological relevance. Studies of the potential dependence of inactivation and reactivation rates for CN^- show clearly that reactivation (ligand OFF) becomes significantly faster under the more reducing conditions that would favor C_{red2}, whereas inactivation (ligand ON) rates do not depend so much on potential. Comparative numerical data on binding affinities and rates are shown in Tables 3 and 4.

Table 3. K_M and K_i Constants for $CODH_{Ch}$ I and $CODH_{Ch}$ II at 25 °C, pH 7.0, Unless Stated Otherwise[a]

	−209 mV	−560 mV		−760 mV	
	K_M (CO)	K_M (CO_2) (mM)	K_i (CO) (μM)	K_M (CO_2) (mM)	K_i (CO) (μM)
$CODH_{Ch}$ I[b]	2 ± 1	8.1 ± 2.1	46	7.1 ± 0.7	337
$CODH_{Ch}$ II		8.0 ± 1.6	5	6.0 ± 1.0	85

[a]Data cited from ref 144 unless otherwise stated. [b]Data taken from ref 45a, pH 6.0.

Table 4. Comparison of Half-Times for Inactivation by Cyanide$^-$ (0.5 mM) and Reactivation for $CODH_{Ch}$ I and $CODH_{Ch}$ II

	$CODH_{Ch}$ I		$CODH_{Ch}$ II	
potential mV vs SHE	ON $t_{inact(1/2)}$, s^{-1}	OFF $t_{react(1/2)}$, s^{-1}	ON $t_{inact(1/2)}$, s^{-1}	OFF $t_{react(1/2)}$, s^{-1}
+140	83 ± 15		130 ± 25	
−460	95 ± 15		307 ± 75	
−560	95 ± 15	still inhibited	161 ± 16	still inhibited
−660	73 ± 15	143 ± 10		
−760	64 ± 10	19 ± 7	54 ± 3	≪limit of detection

Sulfide is an unusual inhibitor, as it has no effect until the electrode potential is raised hundreds of millivolts above the reversible CO_2/CO potential[−], an observation which shows that sulfide (entering as HS^- or H_2S) does not directly target an active state of CODH but promotes oxidative inactivation at a higher potential.[45b] The fact that the reactivation potential is much lower than that observed without sulfide shows immediately that a different C_{ox} state is being formed, one that probably has a sulfide entity attached (in place of water or hydroxide). A similar reactivation process has been observed in samples of $CODH_{Ch}$ I that have not been deliberately exposed to sulfide during the experiment, suggesting that those samples already contained a sulfide entity. Sulfide binding at the C-cluster and its role in activity has been a controversial issue over many years of studying CODH; the PFE results for $CODH_{Ch}$ I and II now show that sulfide is associated with oxidized forms of the enzyme and may be retained in the active site unless quite reducing conditions are applied.

The fact that the binding abilities of different inhibitors and substrates depend strongly on potential demonstrates a further aspect of catalytic bias that was not implicit in the basic model, which dealt only with substrate-saturated conditions. The potential used to drive the reaction in one particular direction also controls the redox state of the active site prevailing during the catalytic cycle and, hence, its ability to bind a particular agent. The range of potentials over which different substrates and inhibitors CO, CN^-, NCO^-, and HS^- target $CODH_{Ch}$ I is shown in Figure 7. A scheme outlining these conclusions is shown in Scheme 5. Similar results have been obtained for $CODH_{Ch}$ II, suggesting that these features may be characteristic properties of the C-cluster.

The catalytic bias of $CODH_{Ch}$ I and $CODH_{Ch}$ II may now be articulated as follows: First, if binding affinity is ignored, i.e., assuming conditions in which CO or CO_2 levels comfortably exceed their respective Michaelis constants, both $CODH_{Ch}$ I and $CODH_{Ch}$ II are excellent catalysts of CO_2 reduction, a factor that seems to relate to the favorable negative potential at which we suggest that electrons would enter the enzyme via the

dx.doi.org/10.1021/cr400461p | Chem. Rev. 2014, 114, 4149−4174

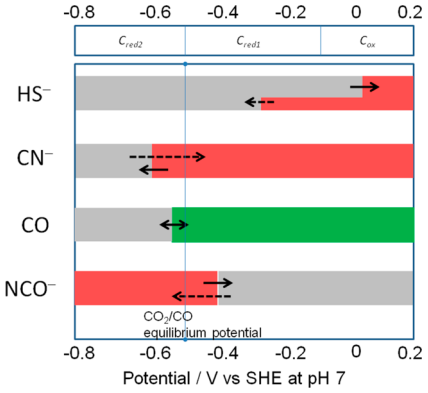

Figure 7. Potential dependence of binding of inhibitors to $CODH_{Ch}$ I. Red refers to the potential region over which the enzyme is inhibited, gray indicates no binding, and green indicates that binding leads to turnover. The dashed arrows indicate reactions that are slow compared to those indicated by full arrows. Reprinted with permission from ref 45b. Copyright 2013 American Chemical Society.

Scheme 5. Summary of the Interceptions of the Catalytic Cycle of $CODH_{Ch}$ I by Small Molecule Inhibitors, As Deduced from PFE Experiments[a]

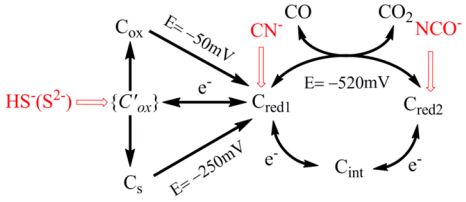

[a]The potentials −250 and −50 mV are the values observed for reactivation of enzyme with and without sulfide. The potential −520 mV is the standard potential for the CO_2/CO half-cell reaction at pH 7.0. Reprinted with permission from ref 45b. Copyright 2013 American Chemical Society.

D-cluster. If electrons could enter only at a much higher potential (in effect a de-energization), CO_2 reduction would not occur. Second, if substrate binding is not ignored, the fact that CO_2 binding is weak and occurs only at the strongly reducing state C_{red2} means that the physiological bias should lie against CO_2 reduction and in favor of CO oxidation; indeed, these enzymes can easily scavenge trace CO. The tighter binding of CO to $CODH_{Ch}$ II compared to $CODH_{Ch}$ I certainly suggests that $CODH_{Ch}$ II should be the better CO scavenger.

The highly active and reversible nature of CODH has stimulated some unusual electrochemical experiments without an electrode, experiments that demonstrate interesting benchmarks for technology. In one set of investigations, molecules of $CODH_{Ch}$ I were coattached with a [NiFe]-hydrogenase (Hyd-2 from *E. coli*) to the surface of graphite particles (platelets formed by grinding pyrolytic graphite with a coarse abrasive) to make a catalyst for the WGS reaction.[51] Aspects of this experiment are shown in Figure 8.

Panel A shows a scheme representing the flow of electrons between the two enzymes across the conducting particle. Panel B shows the voltammograms for $CODH_{Ch}$ I and Hyd-2 enlarged to focus on the regions where the catalytic current for each respective system (50/50 CO/CO_2 and 50% H_2/pH 6) intersect the potential axis. The 0.11 V difference in the two potential values gives the thermodynamic driving force available for the WGS reaction, and the fact that this difference is

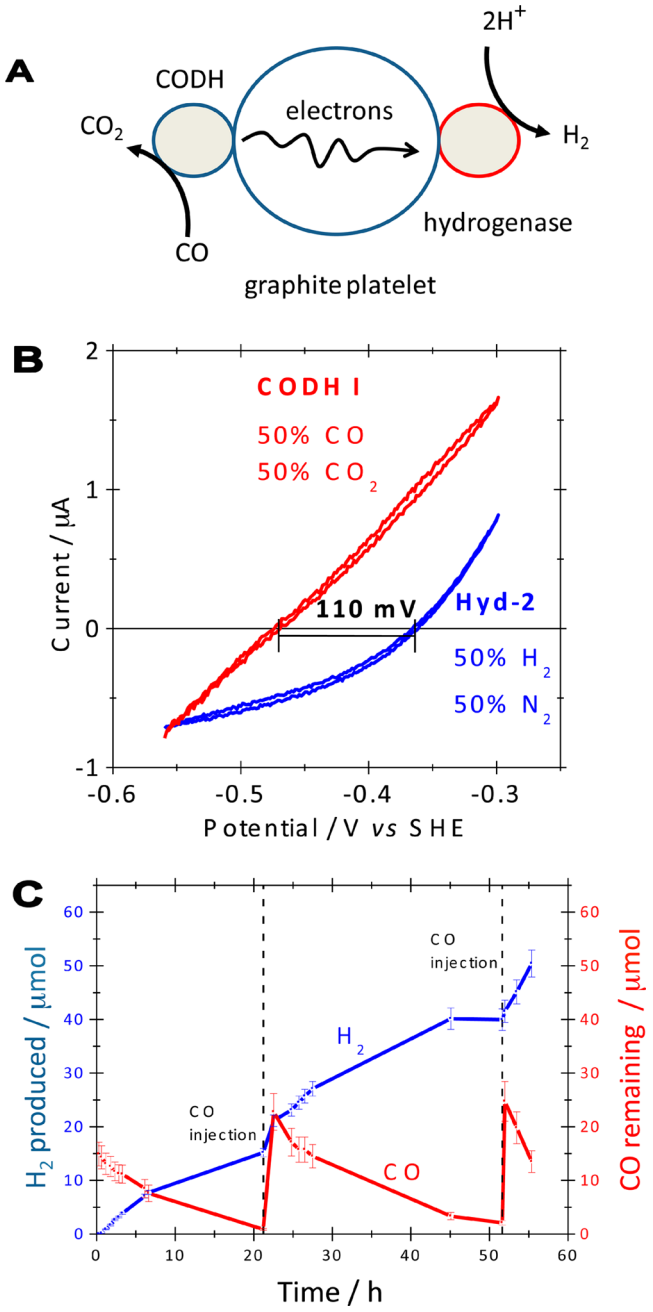

Figure 8. (A) Cartoon representation of an enzymatic device for catalysis of the water−gas shift reaction. Electrons released by CODH-catalyzed CO oxidation are transferred through a graphite particle to a CO-tolerant hydrogenase that reduces protons to H_2. (B) Typical cyclic voltammograms (from separate experiments) showing the reversibility of electrocatalysis by $CODH_{Ch}$ I and a hydrogenase (Hyd-2) from *E. coli*, measured at pH 6.0, 30 °C, scan rate 10 mV s^{-1}, electrode rotation rate 2500 rpm. (C) H_2 production and CO depletion over the course of 55 h at pH 6.0, 30 °C, as quantified by GC analysis. Fresh aliquots of CO were introduced at the times indicated. Adapted with permission from ref 51. Copyright 2009 American Chemical Society.

displayed so sharply is due to the fact that these enzymes are reversible electrocatalysts. The particles were then suspended in aqueous solution under an atmosphere of CO, and the gas composition was measured at different time intervals by gas chromatography. The graphite particle conducts electrons produced from the oxidation of CO by CODH to Hyd-2,

dx.doi.org/10.1021/cr400461p | *Chem. Rev.* 2014, 114, 4149−4174

which converts H^+ to H_2. Details of the experiment are shown in panel C, which shows how CO depletion corresponds to the simultaneous formation of H_2. After CO is exhausted, recharging the vessel with more CO restarts H_2 formation.

On the basis of the amount of enzyme attached to the particles and the ambient temperatures used, the suspension gives a higher rate of H_2 production than industrial catalysts: for example, a homogeneous catalyst $Ru_3(CO)_{12}$ is reported as having a WGS reactivity of 0.01 (mol H_2) s^{-1} (mol catalyst)$^{-1}$ at 160 °C, and Au−CeO_2 nanomaterials, regarded as being highly efficient heterogeneous catalysts, show turnover frequencies up to 3.9 site^{-1} s^{-1} at 240 °C. The data correspond to an average H_2 production rate of 2.5 (mol H_2) s^{-1} (mol adsorbed Hyd-2)$^{-1}$ and a CO depletion rate of 0.07 (mol CO) s^{-1} (mol adsorbed CODH I) s^{-1}. The rates per enzyme molecule are lower limits because it is assumed that all the adsorbed enzyme is electrocatalytically active. The empirical turnover frequency is based on the less active component, i.e, Hyd-2, and therefore, the particles display an equivalent per "site" WGS turnover frequency of at least 2.5 s^{-1} at 30 °C. Importantly, significant rates of WGS conversion by this system are even detectable at ice temperature. Finally, referring back to Figure 7, we note that requirement for even a modest (0.1 V) overpotential for onset of CODH or hydrogenase activity would result in no WGS activity being observed.

$CODH_{Ch}$ I and II also have been studied to assess the possibilities for artificial photosynthetic CO_2 reduction. The aim has been to use the enzyme, with its superb efficiency, to establish what should be possible using semiconducting materials to harvest light and generate excited electrons, analogous to photosystem I, the fuel-forming complex of natural photosynthesis.[145] One requirement of the semiconductor is that the conduction band into which the electrons are injected has a potential E_{CB} that is sufficiently negative to reduce CO_2 to CO. The principle is represented in panel A of Figure 9.

The first of experiments used $CODH_{Ch}$ I attached to various nanoparticles for which the natural band gaps E_G exceed the energy available from visible light; consequently, the nanoparticles were modified by coattachment of the photosensitizing complex "RuP" = $[Ru^{2+}(bpy)_2(4,4'\text{-}(PO_3H_2)_2\text{-}bpy)]^{2+}$ (λ_{max} 455 nm), analogous to technology introduced by Michael Grätzel for dye-sensitized photovoltaic cells.[146] The relevant conduction band potentials E_{CB} (measured for bulk materials) are as follows: TiO_2 (anatase), −0.52 V (note E_{CB} = 3.1 eV, hence the need to use UV irradiation when RuP is not coattached); TiO_2 (rutile), −0.32 V; ZnO, ca. −0.5 V; $SrTiO_3$, −0.72 V. For comparison the standard reduction potential for the CO_2/CO couple at pH 6.0 is −0.46 V.

The results depicted in panel B show that CO production by dye-sensitized visible light excitation depends greatly on the nature of the metal oxide semiconducting nanoparticles. Anatase is clearly supreme: the nanoparticles known as P25 are a composite of anatase with some rutile phase, although rutile itself is inactive (as expected, since E_{CB} is too positive to drive CO_2 reduction) and $SrTiO_3$ is possibly inactive because E_{CB} is so negative that electrons easily transfer back to RuP. The best rate, obtained with P25 and calculated on the basis of total $CODH_{Ch}$ I used, equates to a CO production rate of approximately 0.15 s^{-1} per molecule of CODH.[147] This rate is much slower than that achieved for a hydrogenase at the same material (50 s^{-1}), a fact that is still not resolved. One important difference between the conventional electrochemical and photoexcitation experiments is that, in the latter, electrons may recombine before being used by the catalyst. The tentative conclusion is that a good photoelectrocatalyst should be one that traps *all* the electrons required to carry out the reaction and restricts their return to the semiconductor and inevitable recombination.

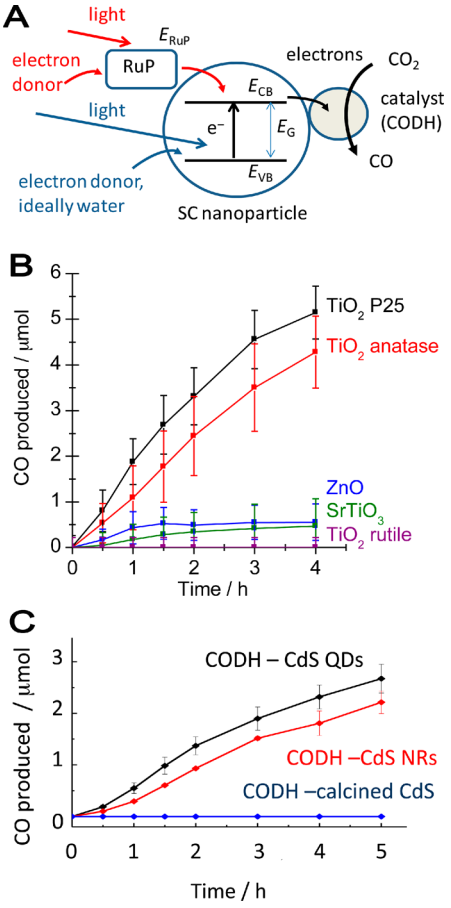

Figure 9. Photoelectrocatalysis of CO_2 reduction to CO catalyzed by CODH attached to light-harvesting nanoparticles. (A) The concept: red arrows correspond to injection of electron into the conduction band (potential E_{CB}) by a photosensitizer (RuP) attached to the nanoparticle; green arrows correspond to injection of electron into the conduction band by band gap excitation (potential difference E_G) from the valence band (potential E_{VB}). The hole in either dye or valence band must be filled more rapidly than the electron can return (the electron−hole recombination rate). (B) Production of CO by visible light using a photosensitizer. Experiments carried out by irradiating a vial containing a 5 mL suspension of various semiconducting nanoparticles with visible light (λ > 420 nm). In each case, 5 mg of nanoparticles (20 mg in the case of ZnO) was modified with $CODH_{Ch}$ I (total 2.56 nmol) and RuP (total 56 nmol). The buffer in each experiment was 0.20 M MES, pH 6, 20 °C. (C) Production of CO by visible light using direct band gap excitation of various types of cadmium sulfide attached to $CODH_{Ch}$ I. QD = quantum dot, NR = nanorod; calcined CdS was heated at 450 °C for 45 min. The buffer in each experiment was 0.35 M MES, pH 6, at 20 °C. Adapted from refs 147a (copyright 2011 The Royal Society of Chemistry) and 148 (copyright 2012 The Royal Society of Chemistry) with permission.

Using semiconducting materials with a smaller band gap, it is possible to use visible light with the need for dye sensitization. Experiments similar to those with RuP-modified anatase, but using band gap excitation, were carried out using different types of nanoparticle formed from cadmium sulfide, CdS. As a rough

dx.doi.org/10.1021/cr400461p | *Chem. Rev.* 2014, 114, 4149−4174

guide, for bulk CdS, E_g = 2.3 eV (corresponding to λ = 540 nm) and E_{CB} = −0.87 V. Using CdS nanoparticles (nanorods, NR) or CdS quantum dots (QD), slightly higher rates were achieved, 0.25 s^{-1} compared to the results obtained with anatase (panel C).[148] The CdS quantum dots have a typical radius that is half that of CODH; thus, in principle, up to 10 QDs may bind to one CODH molecule, reversing the size ratio indicated in panel A. Thermal calcination of CdS nanoparticles, which results in irregular clusters of larger particle size, resulted in no activity when CODH was attached.

The success of these artificial photosynthesis experiments gives strong encouragement for pursuing research in this area and for the role that enzymes play in providing a reversible catalyst in which many different properties can be modified by genetic engineering and tested quantitatively by electrochemical methods.

3. ACETYL-COA SYNTHASE

3.1. Chemistry and Biochemistry of C−C Bond-Forming Reactions Involving CO_2 and CO

Developing an industrial process that efficiently couples CO_2 reduction to CO with a carbonylation reaction would be an important advance in the chemical industry because carbon−carbon formation by reactions with CO is instrumental in many industrial processes.[149] CODH/ACS catalyze such a coupled process as an important component of the biological carbon cycle.[46] If fuels could be made from CO_2, these C−C bond-forming reactions will be of even more importance in energy generation.

Industrial processes involving carbonylation chemistry include the Monsanto process, hydroformylation, and the Reppe process. As has been pointed out elsewhere,[150] the intermediate steps in the Monsanto process for acetic acid formation from methanol and CO are nearly identical to those in the catalytic mechanism of ACS, as described in the Introduction. Both the biological and homogeneous catalysts use organometallic mechanisms that feature low-valent metal centers [e.g., Rh(I) vs Ni(I)] to react with CO and form a metal−carbonyl bond (M−CO) or with a methyl donor and generate a methyl−metal bond (M−CH_3). The key carbon−carbon bond-forming reactions involve a migratory insertion of the metal-bound CO and methyl groups to generate an acyl−metal intermediate that undergoes reductive elimination by a coordinated iodide in the chemical reaction or by the thiolate of CoA in ACS to generate acetyl-CoA.[151] Acetyl-CoA then serves as a source of energy and cell carbon.[30] M−alkyl and M−CO are also key intermediates in the hydroformylation reaction, to convert alkenes to aldehydes. Similar organometallic intermediates are formed in the Pd-based Reppe process.[31b]

3.2. Characteristics of CODH/ACS

3.2.1. Enzymatic Activity. The gene encoding ACS (*acsB*) is a marker for the Wood−Ljungdahl pathway, and whenever it occurs in a microbial genome, it is within a gene cluster containing other pathway genes.[41] ACS associates tightly in a complex with CODH and utilizes the product of the CODH reaction (CO) as its substrate in a kinetically coupled reaction linked to generation of acetyl-CoA via eq 11.[61,71b,152] The second substrate of ACS is a methyl group donated by a methylated B_{12} protein, the corrinoid iron−sulfur protein (CFeSP). The third substrate is CoA, which reacts with CO and the Co-bound methyl group to make acetyl-CoA, a cellular carbon and energy source.

As shown in Figure 1, ACS can catalyze this reaction reversibly. Thus, in aceticlastic methanogens, it catalyzes the disassembly of acetyl-CoA, breaking both the C−C and C−S bonds to form CoA, the methylated CFeSP, and CO.[153] A convenient assay for ACS is to measure that rate of exchange of ^{14}C from [1-^{14}C] acetyl-CoA with ^{12}CO. For ACS (ACS_{Ch}) and CODH/ACS (CODH/ACS_{Ch}) from *C. hydrogenoformans*, exchange rates were reported to be 2.4 or 5.9 μmol of CO per min per mg, respectively, at 70 °C and pH 6 in the presence of 3 mM Ti(III) citrate.[110] The exchange rate reported for CODH/ACS_{Mt} is 0.16 μmol of CO per min per mg at 55 °C and pH 6, without addition of any external reducing agent.[154] ACS_{Ch} and CODH/ACS_{Ch} also catalyze acetyl-CoA synthesis from CFeSP, methylcobalamin, CoA, and CO with activities of 0.14 and 0.91 U/mg μmol of acetyl-CoA production per min per mg.[110]

$$CO + CH_3{-}Co{-}CFeSP + CoA \rightarrow CH_3{-}CO{-}CoA + CFeSP \quad (11)$$

3.2.2. Active Site Metal Cluster and the Importance of Nickel in ACS. The active site of ACS, so-called the A-cluster, was the first NiFeS cluster reported,[155] although the specific role of nickel in ACS activity was established later.[156,157] In the A-cluster, a Fe_4S_4 cluster is bridged to a nickel, called the proximal nickel (Ni_p) because of its proximity to the cluster, and also thiolate-bridged to the distal nickel (Ni_d), which is coordinated by two cysteine and two backbone amides as shown in Figures 10 and 11. The Ni_d, stabilized due to its square planar geometry and oxidation state (2+), is adjacent to a cavity that can accommodate the substrate and products. Ni_p is coordinated by three S atoms in an apparent T-shaped environment. Another ligand, which completes a distorted square planar coordination, has been assigned as an oxygen ligand donated by water[110] or an acetyl[39a] group, though, in the

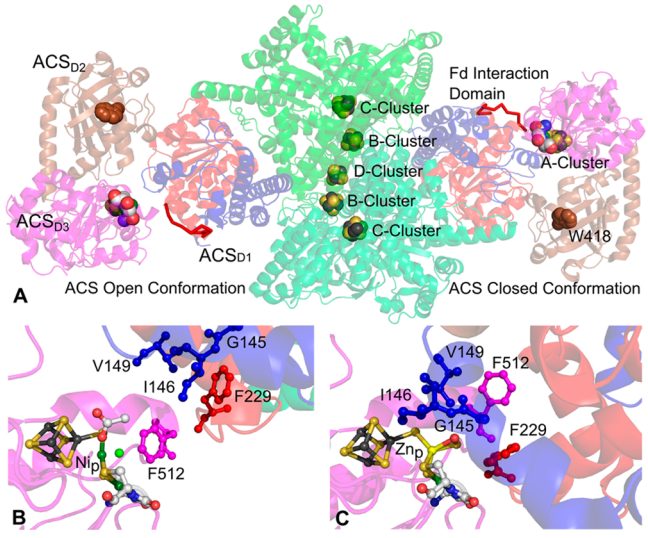

Figure 10. Structure of CODH/ACS_{Mt}. (A) Overall structure of CODH/ACS. Green units in the center are the two CODH homodimers; the left unit is the ACS in open conformation, and the right unit is the ACS in closed conformation. Closer views of the A-cluster pocket in (B) open conformation and (C) closed conformation. Atom colors: Brown (iron), orange (sulfide), red (oxygen), blue (nitrogen), light green (carbon), dark green (nickel), white (unassigned). Generated using Pymol from PDB 1OAO.

dx.doi.org/10.1021/cr400461p | Chem. Rev. 2014, 114, 4149−4174

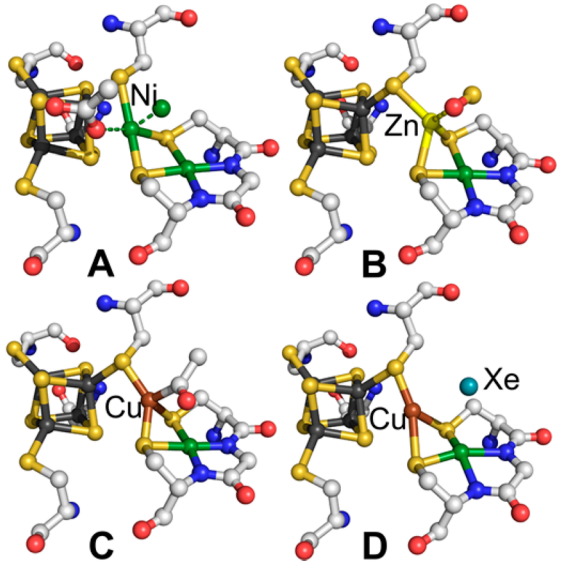

Figure 11. Structure of A-cluster from PDB (A and B) 1OAO, (C) 1MJG, and (D) 2Z8Y. Generated using Pymol.

latter case, the structure was of an enzyme containing Cu at the Ni_p site. The Ni_p is labile (i.e., easily replaced by other metals) and is thought to be the sole metal that is directly involved in binding the substrates. Two different crystal structures showed copper or zinc located at the Ni_p site (Figure 11),[39a,b] and early studies indicated a positive correlation between the copper content and ACS activity; thus, copper was suggested to be a component of the active cluster.[158] However, studies over a much wider range of Ni contents demonstrated that activity was positively correlated with Ni and negatively related to the Cu content;[110,159] furthermore, copper was not responsible for, and even inhibited, the activity of the enzyme.[160] The active methanogenic enzyme was shown to contain two Ni per active center. Thus, it is clear that the active A-cluster contains two Ni and four Fe atoms. In almost all of the studies utilizing recombinant ACS, the enzyme is activated by nickel reconstitution. CO binding to the A-cluster upon the reduction by dithionite results in an EPR-active species called NiFeC species, due to its hypefine broadening by ^{61}Ni, ^{57}Fe, and ^{13}CO, and is used to determine the nickel incorporation into the A-cluster.

3.3. Structure of the CODH/ACS

3.3.1. Inner Channel in CODH/ACS. The gene encoding ACS is generally contiguous with that encoding CODH. This genetic linkage parallels tight enzymatic coupling of CODH and ACS. Kinetic coupling has been established by several experiments, including one in which CO_2 was used as a substrate and the incorporation of in situ-formed CO into the carbonyl group of acetyl-CoA was monitored. Unlabeled CO in solution does not decrease the rate or extent of incorporation of labeled $^{14}CO_2$ into acetyl-CoA.[161] Although CO is a substrate for the CODH/ACS, absence of CO in the solution did not affect acetyl-CoA synthase activity, while CO_2 had a major impact on the reactivity.[63] Similarly, addition of hemoglobin or myoglobin to the assay mixture as a CO scavenger only marginally inhibited acetyl-CoA synthesis.[63,161] These and other results[63,161,162] suggest that CO produced in the CODH subunit from CO_2 remains sequestered within the enzyme without equilibrating with solution as it is transferred to the ACS active site, and it was proposed that CO migrates through an inner channel within the CODH/ACS complex from the CODH to that ACS active site.[63,161]

The crystal structure of $CODH/ACS_{Mt}$ showed that the A- and C-clusters are separated by 67 Å, which would seem to be too long to allow kinetic coupling of the CODH- and ACS-catalyzed reactions (Figure 10A).[39] However, interior surface calculations and diffraction experiments on Xe-treated crystals disclosed the presence of a continuous 140 Å long hydrophobic tunnel that connects the active sites of CODH and ACS, the C- and A-clusters, respectively (Figure 12).[39,71e] Since the van de

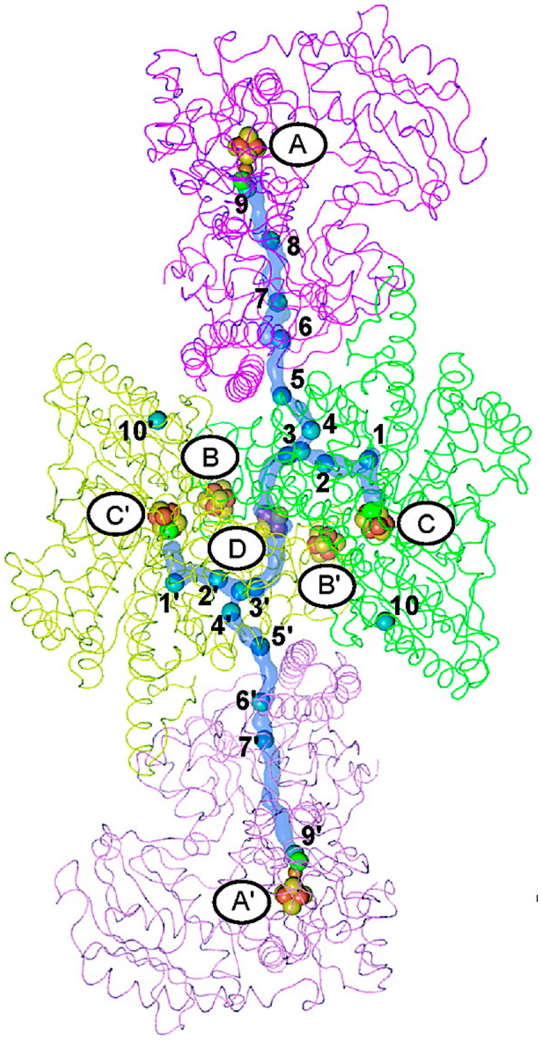

Figure 12. Structure of $CODH/ACS_{Mt}$ crystallized in the presence of high pressures of Xe (PDB 2Z8Y) (shown as the blue spheres) to reveal the hydrophobic CO tunnel. Adapted with permission from ref 71e. Copyright 2008 American Chemical Society.

Waals radius of Xe (2.16 Å) and CO (~2 Å) are similar, Xe can be considered as a good mimic for CO. A total of 19 Xe atoms were located in this hydrophobic tunnel. Examination of the residues within 5 Å of Xe atoms shows an insignificant degree of sequence homology but supports a highly conserved pattern of hydrophobic residues (except for the positions and orientations of C468 and T593, which are located near the C-cluster). The tunnel is composed of a series of interconnected hydrophobic pockets that can be conceptualized as a pinball plunger where launching of each ball (gas molecule) from the trough into the playfield releases another ball into the

dx.doi.org/10.1021/cr400461p | Chem. Rev. 2014, 114, 4149–4174

launching lane. Of course, with CODH/ACS, multiple balls are at play in the channel and each has only one target, the A-cluster. In each of the ACS subunits, one Xe atom was found 3.5 Å from Ni_p (Figure 11D). Further experimental support for a CO-binding pocket near the A-cluster is the finding that, when CO-bound ACS is subjected to photolysis, the energy barrier for recombination of Ni_p with CO is only 1 kJ/mol.[163]

When residues (A578, L215, A219, A110, A222, A265) that are located within the hydrophobic channel in $CODH/ACS_{Mt}$ were substituted, ACS activity with CO_2 as substrate was severely diminished.[164] These results support the importance of the tunnel for CO migration to the A-cluster. Furthermore, the variants exhibit little inhibition of acetyl-CoA synthesis by CO, in contrast to the wild-type proteins, indicating that the channel plays an important role in cooperative inhibition of A-cluster activity by CO. It was suggested that there may be at least two ways for CO to reach the A-cluster: through the channel and from the solvent. A water channel close to the $\beta\beta$ interface is proposed to be the second way for the CO,[164a] but this idea is not well established yet.

The role of the CO channel is most likely to prevent the loss of energetically expensive CO in the solution and to efficiently direct this gaseous substrate to its site of reactivity at the A-cluster.

3.3.2. Conformational Changes. As shown in Figure 10, ACS consists of three main domains. The first domain, which interacts with CODH, starts with helices and continues with a Rossman fold. This domain contains a ferredoxin interaction domain.[165] The second domain includes six Arg residues near Trp418 (Figure 10A). These residues are involved in CoA binding according to fluorescence-quenching studies of Trp418 and inhibition studies of CoA binding upon modification of Arg residues.[166] The final domain bears the A-cluster. This domain undergoes structural rearrangements during turnover (Figure 10B,C).

ACS binds three substrates of vastly different sizes: CO (30 Da), CoA (770 Da coenzyme), and methylated CFeSP (88 kDa dimeric protein). $CODH/ACS_{Mt}$ is crystallized in two different forms that are thought to be related to the catalysis: closed[39a] and open[110] conformations. Another structure depicts both conformations (one in each CODH/ACS dimer) (Figure 10).[39b] In its closed conformation, the channel is open, allowing CO to pass through the tunnel to the A-cluster; however, there is no apparent access to the methylated CFeSP. In the open configuration, one of the domains (domain 3) of ACS rotates, which partially exposes the A-cluster, enabling interaction with the CFeSP and closure of the CO tunnel.

Although the catalytic importance and the main trigger of this conformational change are not yet well established experimentally, there appear to be at least four discrete conformations. Throughout all of these conformational changes, both CO and the A-cluster must be protected from exposure to solvent, because CO does not equilibrate with solvent during catalysis.[161,63] In one closed conformation, poised for binding CO, the CO channel is open to allow the CO to reach the A-cluster, which is buried and unable to access the CFeSP (Figure 10C). In an open conformation, ready to bind the methyl group, the A-cluster is rotated to interface with the CFeSP and the CO channel is blocked to avoid CO release (Figure 10B). Another closed (solvent-excluded) conformation is required during formation of the acetyl–metal complex to avoid hydrolysis of the acetyl–metal center. Then, the A-cluster must be rotated into a more open conformation to allow CoA binding, thiolytic cleavage of the acetyl group, and acetyl-CoA release. A crystal structure of the truncated ACS_{Mt} is proposed to represent the CoA binding conformation of the enzyme.[167] While there is concrete crystallographic proof for the first two conformations, more work is needed to reconcile the other two conformations.

Experiments performed on the methanogenic acetyl-CoA decarbonylase/synthase (ACDS) suggested that the N-terminal region of ACS is involved in C–C bond cleavage.[168] On the basis of kinetic and spectroscopic data for different ACS enzymes, it appears that conformational changes directly impact stability of the Ni–acetyl intermediate. Steric hindrance around the Ni_p due to conformational changes of a proximal phenylalanine (F512) is proposed to facilitate C–C bond cleavage and to affect interaction of CO with the enzyme.[169] Thus, conformational changes clearly affect ACS enzymatic activity, and studies are needed to better understand these impacts on the catalytic mechanism.

3.4. Catalytic Mechanism of Acetyl-CoA Synthesis

The chemistry of the ACS reaction is catalyzed by the A-cluster; surprisingly, even though this center contains six redox-active metals, substrate binding seems to be confined to a single metal center, Ni_p. Pulse-chase studies indicate that the steady-state mechanism involves random order binding of the methyl group and CO, followed by ordered binding of CoA.[170] The two competing mechanisms that have been proposed differ in the oxidation state of the Ni_p. The "paramagnetic mechanism" proposes a $Ni_p(I)$ catalyst and Ni(I)–CO [or methyl–Ni(III) and methyl–Ni(II) for the other branch of the random mechanism] and acetyl–Ni(II) intermediates (Scheme 6),[171]

Scheme 6. Proposed Paramagnetic Mechanism of Acetyl-CoA Synthesis Catalyzed by the A-Cluster

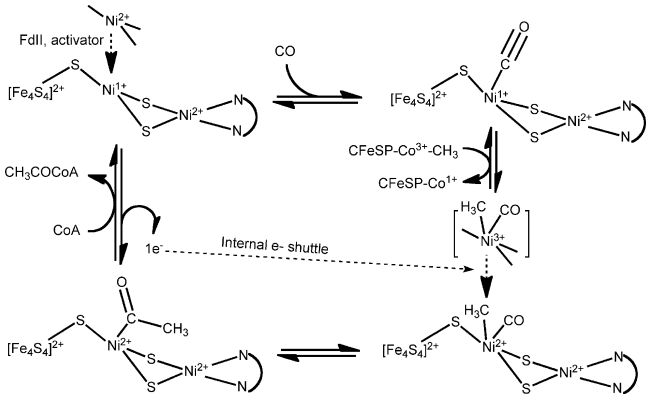

while the "diamagnetic mechanism" proposes a Ni(0) active catalyst with Ni(0)–CO and methyl–Ni(II) [without the paramagnetic methyl–Ni(III)] intermediates.[115] However, both mechanisms include organometallic methyl–Ni, acetyl–Ni, and thiolytic cleavage of the acetyl–Ni species by CoA. Because of their similarity, we will focus here on the paramagnetic mechanism and include relevant aspects of the Ni(0)-based mechanism. As described elsewhere, the mechanism of acetyl-CoA formation resembles the Monsanto process, where acetic acid is produced by the reaction of methanol and CO on a rhodium complex through organometallic complexes.[172,173]

The essential role of the tetrameric $\alpha_2\beta_2$ CODH (as it was known until 1985) in acetyl-CoA synthesis was predicated on

dx.doi.org/10.1021/cr400461p | Chem. Rev. 2014, 114, 4149–4174

studies of the isotope exchange reaction between CO and the carbonyl group of acetyl CoA.[152] In this reaction, the C−C and C−S bonds of acetyl-CoA are cleaved to generate enzyme-bound methyl, carbonyl, and CoA groups, allowing the central carbonyl group to exchange with free CO; finally, the C−S and C−C bonds must be resynthesized. That CODH/ACS alone (and it was subsequently shown that ACS alone is required for this reaction[61]) is required clearly demonstrated that this enzyme is responsible for the key step in the Wood−Ljungdahl pathway: condensation of methyl, CO, and CoA to form acetyl-CoA. Because CODH/ACS catalyzes an exchange reaction between CoA and acetyl-CoA much faster than the CO/acetyl-CoA exchange reaction, CoA was proposed to be the final substrate that reacts with the bound acetyl group to form acetyl-CoA.[174] Since methylation of CODH/ACS by the methylated CFeSP can occur without any CO or CoA and also faster than the overall acetyl-CoA synthesis reaction, the methyl group was suggested to be the first substrate to bind Ni_p.[175−178] Since the back-π-donation upon CO binding to the metal is expected to decrease the electron density on the metal center, its reactivity with methyl could be decreased if methyl is bound as the second intermediate. However, CO can also bind the enzyme in the absence of a methyl donor or CoA; furthermore, a pulse-chase study of acetyl-CoA synthesis with $CODH/ACS_{Mt}$ and with ACS-only clearly indicated that either CO or methyl can bind first during catalysis.[170] In this pulse-chase (or isotope dilution) study, $CODH/ACS_{Mt}$ is incubated with equimolar amounts of a labeled substrate ($^{14}CH_3$−CFeSP, ^{14}CO, or 3′-dephospho-CoA) and then mixed with a solution containing either (1) the other two substrates at high concentrations or (2) all three substrates at high concentrations. Incorporation of the label into product is measured. If the mechanism is strictly ordered with labeled substrate being first to bind, addition of that unlabeled substrate in excess will not lead to dilution of the isotope. On the other hand, if it is actually the second substrate in the sequence, it must dissociate to allow the true first substrate to bind before it can form a productive complex. Dissociation leads to isotope dilution, as detected in the product. This method is valuable because one can determine how ordered (or how random) the reaction is. Nearly complete dilution of dephospho-CoA in the pool of excess CoA is observed. However, there is no measurable isotope dilution when ACS is treated with $^{14}CH_3$−CFeSP or ^{14}CO. Thus, the first substrate can be either the methyl group or CO group, and the third substrate is CoA. However, it is important to note that CO but not CO_2 was used as the source of the carbonyl group of acetyl-CoA; thus, possible regulatory effects of the tunnel and the possible effects of the coupled reaction on the mechanism were not addressed in this study.

For illustration, we show the mechanistic scheme as an ordered reaction with CO as the first binding substrate (Scheme 6). Before substrate binding, a reductive activation by Ti(III) citrate or another low-potential electron donor is required. The oxidized state of the A-cluster, which has a configuration of $[Fe_4S_4]^{2+}Ni_p^{2+}Ni_d^{2+}$, cannot accept a methyl from the CFeSP[177,179] or bind CO.[178] This $Ni_p(I)$ intermediate was trapped by photolysis of the Ni(I)−CO species and its EPR spectrum was recorded, exhibiting g-values of 2.56, 2.10, and 2.01.[163] Then, in a kinetically coupled reaction, $Ni_p(I)$ binds CO as the first step in the mechanism. For this to occur, the tunnel must be open to allow migration of the CO that is produced from CO_2 in the C-cluster. Two reduced states have been observed by Mossbauer spectroscopy: $[Fe_4S_4]^+$ $[Ni_p]^+$ and $[Fe_4S_4]^{2+}$ $[Ni_p]^+$.[180] The Ni_p−CO species is proposed to form the well-characterized NiFeC species.[30] DFT calculations combined with EPR,[155] ENDOR,[181] Mossbauer,[85b,182] IR,[183] and X-ray experiments[184,185] indicate that NiFeC species consists of a $[Fe_4S_4]^{2+}$ cluster bridged to a dinuclear Ni center, Ni_p^+−CO, and Ni_d^{2+}.[186] According to the EPR spectral properties, the unpaired electron density is delocalized over the Ni_p, the $[Fe_4S_4]$ cluster, and the terminal carbonyl group.[155,187]

Various experiments indicate the catalytic competence of the NiFeC species. It forms at the same rate and decays 6-fold faster than the steady-state rate of acetyl-CoA synthesis.[178] The rate of the formation of NiFeC species monitored by EPR equals the rate of the Ni−CO bond formation probed by IR, indicating that Ni−CO is the only metal−carbonyl species formed upon the reaction of ACS and CO.[183b] Controlled potential enzymology studies revealed the need for only a single electron transfer with a midpoint potential of −511 mV[188] to activate the A-cluster, a value that is very similar to that reported for the formation of NiFeC species from acetyl-CoA (−541 mV).[189] Ferredoxin-II (Fd-II), which enhances the isotopic exchange rate,[155] is shown to activate the A-cluster most likely by forming this Ni^+ species.[188]

In the diamagnetic mechanism, formation of a Ni(0) intermediate is proposed[115] and is supported by the ability of a model Ni(0)−phosphine complex to accept a methyl group from a Co^{3+}−CH_3 complex;[190] however, a Ni(0) state on ACS has never been observed or reported. Furthermore, two-electron reduction of Ni(0) to Ni^{2+} would be extremely difficult, since even the reduction potential for Ni^{2+}−CO/Ni^+−CO is already very negative, below −550 mV. The presence of a Ni(0) in a highly electropositive environment formed by Ni_d^{2+} and $[Fe_4S_4]^{2+}$ seems unlikely because electron transfer to the cluster or the Ni_d would be favored.

The second step of the mechanism is binding of the methyl group to the A-cluster. In this step, the protein is most likely in its open conformation, where the A-cluster is accessible to the large CFeSP. Rapid kinetic studies utilizing a chiral methyl donor suggested the transfer of a methyl cation through an S_N2 mechanism where Ni_p attacks to the Co^{3+}−CH_3 on the CFeSP to leave behind a Co^{1+} and a methylated Ni_p. The methyl, like CO, appears to bind to the Ni_p.[156,159,191] Although a radical methyl transfer is suggested according to the model studies,[192,193] this is not feasible in biology, since the reduction potential of Co^{3+}−CH_3/Co^{2+}−CH_3 is below −1 V, which would be too low for physiological electron transfer.[194]

Rapid kinetic studies indicate that both methylated[178,191] and acetylated ACS[195] species are EPR-silent. This represents a challenge for the paramagnetic mechanism, since the S_N2 addition of methyl cation to the Ni_p^+ should result in a Ni_p^{3+}. However, since the Ni_p^{3+} state is predicted to be highly oxidizing and unstable, it should readily be reduced to the Ni^{2+} state. Since acetyl-CoA synthesis does not require net electron transfer from the environment,[152] this reduction could be achieved by an internal electron transfer, as shown in Scheme 6. Fd-II is shown to donate an electron to the proposed Ni_p^{3+} intermediate and to accept an electron during the cleavage of the Ni_p−acetyl intermediate, most likely by interfacing with an internal electron shuttle.[188] However, this internal electron shuttle has not yet been identified. Such an internal electron transfer is not necessary for the diamagnetic mechanism, since Ni(0) is converted to Ni^{2+}−CH_3. However, as mentioned above, the diamagnetic mechanism has its own challenges.

dx.doi.org/10.1021/cr400461p | Chem. Rev. 2014, 114, 4149−4174

Scheme 7. Schematic Views of Model Complexes of A-Cluster

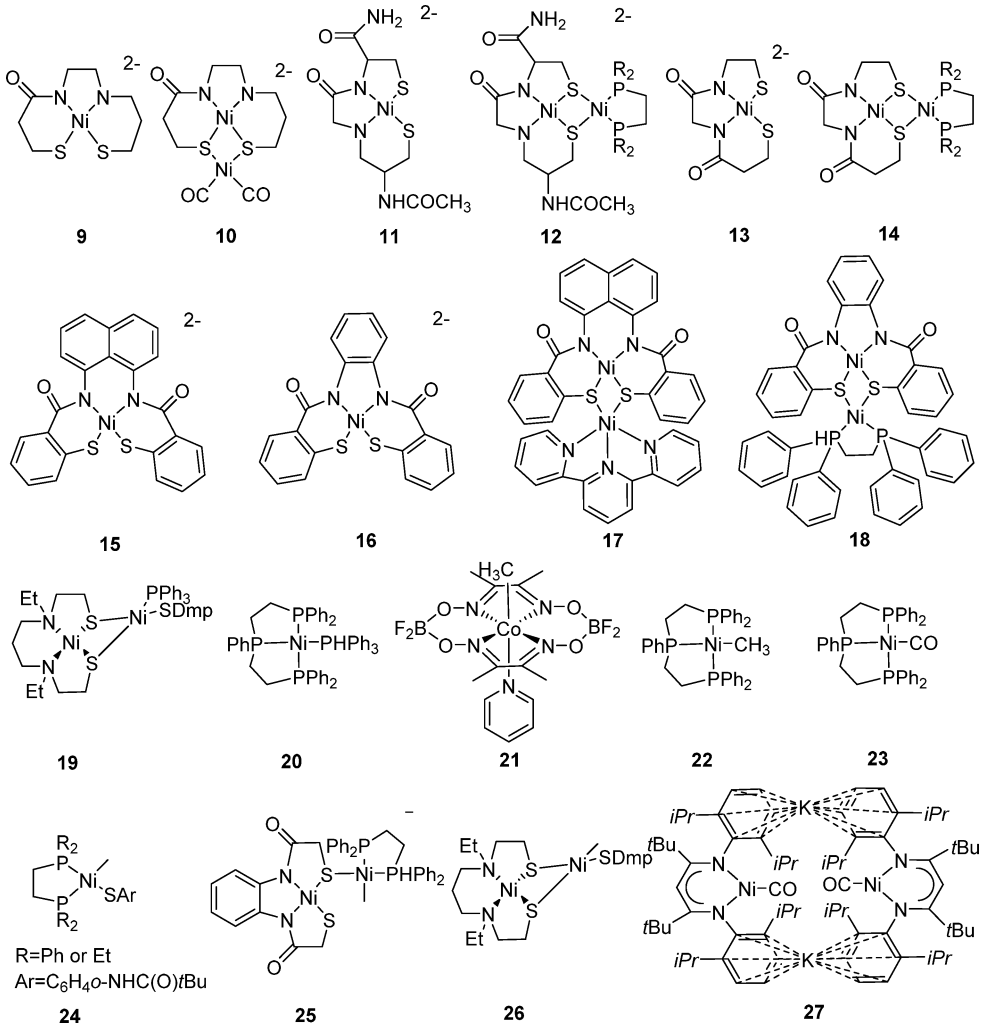

The next step involves a methyl migration (carbonyl insertion) to form an acetyl−metal complex. A crystal structure of ACS_{Mt} is proposed to represent the CoA binding conformation of the enzyme.[167] Addition of CoA is followed by the thiolytic cleavage of the acetyl-CoA product and also the internal transfer of electrons.

3.5. Structural and Functional Models of ACS

Modeling efforts for the A-cluster of ACS up until ~2005 have been reviewed.[196] Thus, we will only briefly cover the Ni complexes reported (Scheme 7).

Since the $[Fe_4S_4]$ complex and the distal Ni are thought to modulate the electronic and redox properties of the active site but not to bind any ligands, most model complexes have focused on imitating the Ni_p or the bimetallic Ni_p−Ni_d environment, omitting the $[Fe_4S_4]$ complex. Initially, compound **10** was prepared by the reaction of **9** with Ni(cyclooctadiene)$_2$ and CO as a very stable complex in anaerobic solution that undergoes immediate degradation upon air exposure.[197] The IR spectrum of **10** exhibits ν_{CO} bands at 1948 and 1866 cm^{-1}. Crystallographic and NMR spectroscopic characterization of the compound indicates the presence of a Ni(0)Ni(2+) couple. The bimetallic Ni complexes, **12** and **14**, have also been reported.[198] Compound **12** was synthesized from the reaction of **11** and $(R_2PCH_2CH_2PR_2)NiCl_2$ (R = Et, Ph). Reaction of **11** with nickel chloride also yielded a trinuclear nickel complex upon the dimerization of two units of **11** around a nickel atom. The Ac−CycGlyCys−$CONH_2$ is used as precursor for the synthesis of compound **11**. Synthesis of compound **12** is a significant improvement, since it includes two sulfides and two phosphines to mimic the environment of Ni_p. That Ni can be reduced to form a Ni(1+)Ni(2+) complex. While the oxidized Ni(II) state cannot bind CO, the reduced state can and be reduced further to the Ni(0)Ni(2+) state. Compound **14**, synthesized from **13**, contains a coordinating ring pattern and donor set for Ni_d that is almost identical to that of the A-cluster. However, no ACS activity or ligand-binding properties were observed for this interesting compound. Furthermore, Harrop reported the synthesis and characterization of new complexes **15**−**18**.[199−201] Treatment of compound **15** with Cu(2,9-dimethyl-1,10-phenanthroline)Cl resulted in a dinuclear Cu(I)−Ni(II) complex, which does not bind CO and does not include a reducible nickel center.[199] Neither compound **15** nor compound **16** can be reduced easily or can bind CO. Compounds **15** and **16** were utilized as precursors to prepare **17** and **18**, respectively. Reduction of **17** with dithionite yields a five-coordinate Ni(I) complex in trigonal bipyramidal geometry with an axial EPR signature of g = 2.226, 2.125. The Ni(I) state of **17** binds CO to form a complex with a rhombic EPR spectra (g = 2.223, 2.218, 2.019), which is typical for six-coordinate Ni(I)−CO complexes[202] and

dx.doi.org/10.1021/cr400461p | Chem. Rev. 2014, 114, 4149−4174

with a Ni(I)−CO band at 2044 cm^{-1}. Compound **18** can be reduced with dithionite or sodium borohydride to form a Ni(I) complex, based on its EPR spectrum. As expected, **18** binds CO in the Ni(I) state, exhibiting a strong Ni(I)−CO band at 1997 cm^{-1}, a value that is very close to what is observed in A-cluster (1996 cm^{-1}).[150] These studies show the stability and inertness of Ni_d^{2+} and reducibility and ligand affinity of the Ni_p atom. A Ni(II)−Ni(I) compound, **19**, was recently shown to accept methyl from methylcobaloxime and form thioester upon CO exposure.[203] This result indicates that a Ni(II)Ni(I) can afford the chemisty of the acetyl-CoA synthesis reaction in a proper coordination and electronic environment.

Reactivity of a $Ni_p(0)$ analogue, Ni(triphos)(PPh_3) (compound **20**), with a methyl−CFeSP analogue, **21**, yields compound **22**.[204] While compound **20** was methylated by **21** in approximately 1 h, no methylation or acylation was observed for compound **23**, even 24 h after of reaction. Furthermore, reaction on compounds **24** and **25** with **21** and CO leads to acetylation of the S-ligand of the methylated nickel and dissociation of the thioester.[205,206] The viability of the Ni(II)/Ni(0) couple in Ni−acyl formation is further supported by another binuclear nickel compound, **26** (Dmp is 2,6-dimesitylphenyl), which forms the acetyl thioester upon reaction with CO.[207] The methyl group in compound **26** was donated either by compound **21** or MeI. These studies support the plausibility of the methyl ligand binding to the metal before CO binds. Similarly, a Ni(0)−CO complex, compound **27** was prepared and shown to accept methyl and to exhibit Ni−acyl bond formation.[208]

As summarized above, inorganic model studies suggest that Ni(II) centers mimicking Ni_d are not reducible or catalytically active. Ni(0) and Ni(I) complexes can bind CO as well as mimic ACS activity. There are also examples of both Ni(I) and Ni(0) complexes that bind methyl followed by CO and vice versa. Further studies are necessary to clarify these mechanistic issues. Inclusion of the Fe_4S_4 cluster in the inorganic models would provide important information about the role of this redox-active center in the ACS reaction and perhaps would afford new catalysts to afford acetyl-CoA synthesis without enzymes.

4. CONCLUSIONS AND FUTURE DIRECTIONS

We have described studies on two remarkable metalloenzymes that have defined novel biochemical mechanisms involving organometallic chemistry to catalyze their reactions. CODH catalyzes CO_2 reduction, a reaction that has important potential impact on the generation of energy-rich compounds and on the environment due to its involvement in the global carbon cycle. This is a catalyst that has optimized its kinetics and thermodynamics, operating at high rates and without an overpotential. These characteristics warrant further studies of CODH aimed at understanding the principles that guide these two enviable properties. Past studies outlined here have uncovered novel metal clusters to bind, activate, and transform substrates (CO and CO_2) and macromolecular channels that enhance flux of precious substrates between catalytic sites. CODH also is a wonderful system to explore how chemical bond forming and breaking interfaces with redox chemistry. Future research will define the kinetic and structural properties and electronic states of the yet-to-capture intermediates in CO oxidation/CO_2 reduction and reveal where the electrons reside during the two-electron redox interconversion. Future studies on this enzyme will be greatly enriched with the development of a well-defined and reproducible way to generate variants of CODH. This enzyme, especially coupled to ACS and other enzymes of the Wood−Ljungdahl pathway, offers great potential for biotechnology through the conversion of simple abundant compounds into needed chemicals and fuels. To realize this promise, host organisms must be developed or reconfigured to foster an anaerobic environment that includes all of the metallochaperones and accessory factors required to support the high activity observed in the native organisms. These factors and their roles need to be characterized.

In order to tap the potential of CODH, ACS must be tamed. Above we have described the highly unusual metal center at the heart of this enzyme and provided information, gleaned by a mixture of biochemical, biological, and biophysical methods, on the modular way that this center forms organometallic (M−CO, M−CH_3, M−acetyl, and M−S) bonds en route to generation of the compound at the center of our metabolic charts, acetyl-CoA. Though we have defined the novel modular approach to synthesis of this key metabolic building block, we do not yet understand the internal redox chemistry that drives C−C and C−S bond formation to generate acetyl-CoA. It is important to capture and characterize the yet undefined intermediates in the ACS catalytic cycle. We have learned to express ACS and reconstitute it in vitro to near full activity; however, the same challenges remain in developing a genetic system that produces a highly active enzyme.

It will be extremely important to understand how the activities of CODH and ACS are coordinated in the complex and to increase our understanding of the dynamics and mechanics of the tunnel that carries CO from the C-cluster to the A-cluster. With both CODH and ACS, it is important to understand the movement of domains and how these proteins interact with other components of the Wood−Ljungdahl pathway, especially the CFeSP.Future high-impact papers will emerge that provide an understanding of the structures of complexes between CODH/ACS and the CFeSP, achievable by X-ray diffraction methods as well as other methods that can define conformational, ligation, and electronic states and measure distances among the redox centers in these various states. Finally, ACS has been found in the multidrug-resistant human pathogen *Clostridium difficile*, and better understanding of these enzymes could foster the discovery of new therapeutic solutions against *C. difficile* infections.[209]

AUTHOR INFORMATION

Corresponding Author

*E-mail: sragsdal@umich.edu.

Notes

The authors declare no competing financial interest.

Biographies

Mehmet Can was born in 1983 in Erzincan, Turkey. He received his B.S. degree in Chemistry in 2006 from Bilkent University (Ankara, Turkey) and his Ph.D. in Chemistry in 2012 from University of Rochester (Rochester, NY) working with Prof. Kara L. Bren. He investigated the factors affecting the heme electronic structure of proteins with heme *c*. In 2012, he joined Prof. Stephen W. Ragsdale's research group at the University of Michigan Medical School (Ann Arbor, MI). He is now working on the key metalloenzymes in the Wood–Ljungdahl pathway, focusing particularly on carbon monoxide dehydrogenase and acetyl-CoA synthase.

Fraser A. Armstrong, Chemistry Professor at Oxford University (Oxford, UK) and Fellow of St John's College (Cambridge, UK), carries out research on the mechanisms of redox enzymes. His group has developed protein film electrochemistry, a powerful suite of dynamic electrochemical techniques for unravelling complex and often intractable electron transfer and catalytic reactions in proteins. Most recently he has focused on mechanisms and exploitation of biological hydrogen, carbon, and oxygen cycling by enzymes, establishing simple demonstrations of photo- and electrochemical devices made possible through the efficiency and selectivity of enzymes, the intention being to inspire and direct bottom-up development of the best chemical catalysts. In 2008, he was elected a Fellow of the Royal Society and has since received the Joseph Chatt Award (2010), the Barker Medal (2012), and the Davy Medal (2012).

Stephen W. Ragsdale is a Professor of Biological Chemistry at the University of Michigan (Ann Arbor, MI). He was born in 1952 and grew up in Rome, GA, He received his B.S. and Ph.D. degrees in Biochemistry from the University of Georgia (Athens, GA), where he began research in microbial biochemistry and enzymology with Dr. Lars Ljungdahl. After graduating in 1983, he was an NIH Postdoctoral Associate with Harland G. Wood at Case Western Reserve University (Cleveland, OH). In 1987, he joined the chemistry faculty at the University of Wisconsin—Milwaukee (Milwaukee, WI), where he was a Shaw Scholar. He joined the Biochemistry Department at the University of Nebraska (Lincoln, NE) as Associate Professor in 1991 and became full Professor in 1996 and Bessey Professor in 2003. In 2007, he joined the faculty at the University of Michigan. His research interests span the areas of microbial and environmental biochemistry, especially as these topics relate to greenhouse gases; metabolic regulation by redox, heme, and CO; metallobiochemistry; and enzymology. He has been studying nickel enzymes, including CO dehydrogenase and acetyl-CoA synthase, for over 25 years and remains intrigued by the remarkable properties of these two enzymes.

ACKNOWLEDGMENTS

Many collaborators, students, and postdoctors have been involved in the work described in this review. S.W.R. is extremely grateful for their intellectual and experimental contributions to our studies of CODH and ACS. Most of their names appear in the cited papers. My laboratory has always been very interactive, so I also must thank my colleagues working on other projects. I also gratefully acknowledge the Metals in Biology Gordon Research Conference, which I first attended soon after being awarded my Ph.D. from the University of Georgia. By providing a generous and stimulating venue that fosters the exchange of ideas and the development of fruitful collaborations and friendships in this wonderful area of metallobiochemistry, that meeting has strongly influenced my research career over these many years. I also wish to thank my colleagues and the administrations at the three institutions where I have received strong support and have developed my independent career. This includes the University of Wisconsin—Milwaukee, where I began my independent career, the University of Nebraska, and the University of Michigan. I also owe a very strong debt to the important influences of family, music, and of the ancient traditions related to yoga and spirituality in my development of a person and scientist. These cross-threads have tremendously enriched my life and my research. The work on the mechanism of CO and CO_2 fixation by the Wood–Ljungdahl pathway has been funded continually since 1987 by NIGMS at NIH and I am extremely grateful for that support and for the recent merit award (R37-GM39451).

F.A.A. has been able to develop the field of Protein Film Electrochemistry through generous and continuous funding from U.K. Research Councils (BBSRC and EPSRC Supergen). Special thanks are due to Drs. Alison Parkin, Vincent Wang, and Thomas Woolerton for particularly important experimental contributions that are described in this Review. F.A.A. is a Royal Society-Wolfson Research Merit Award Holder.

REFERENCES

(1) Yergin, D. *The Quest: Energy, Security and the Remaking of the Modern World*; Penguin Press: New York, 2011.
(2) Hall, D. O.; Rao, K. K. *Photosynthesis*, 5th ed.; Cambridge University Press: Cambridge, UK, 1994.
(3) Fuchs, G. *Annu. Rev. Microbiol.* **2011**, *65*, 631.
(4) Ragsdale, S. W.; Pierce, E. *Biochim. Biophys. Acta, Proteins Proteomics* **2008**, *1784*, 1873.
(5) Pollack, H. N. *A World without Ice*; Avery/Penguin Group: New York, 2009.
(6) *Intergovernmental Panel On Climate Change*; Solomon, S., Qin, D., Manning, M., Chen, Z., Marquis, M., Averyt, K. B., Tignor, M., Miller, H. L., Eds.; Cambridge University Press: New York, 2007.
(7) Boyd, P. W.; Jickells, T.; Law, C. S.; Blain, S.; Boyle, E. A.; Buesseler, K. O.; Coale, K. H.; Cullen, J. J.; de Baar, H. J.; Follows, M.; Harvey, M.; Lancelot, C.; Levasseur, M.; Owens, N. P.; Pollard, R.; Rivkin, R. B.; Sarmiento, J.; Schoemann, V.; Smetacek, V.; Takeda, S.; Tsuda, A.; Turner, S.; Watson, A. J. *Science* **2007**, *315*, 612.
(8) Appel, A.; Bercaw, J.; Bocarsly, A.; Dobbek, H.; DuBois, D.; Dupuis, M.; Ferry, J.; Fujita, E.; Hille, R.; Kenis, P.; Kerfeld, C.; Morris, R.; Peden, C.; Portis, A.; Ragsdale, S.; Rauchfuss, T.; Reek, J.; Seefeldt, L.; Thauer, R.; Waldrop, G. *Chem. Rev.* **2013**, *113*, 6621.
(9) Tenhunen, R.; Marver, H. S.; Schmid, R. *Proc. Natl. Acad. Sci. U.S.A.* **1968**, *61*, 748.
(10) Cobb, N.; Etzel, R. A. *J. Am. Med. Assoc.* **1991**, *266*, 659.
(11) Hampson, N. B.; Weaver, L. K. *Undersea Hyperbaric Med.* **2007**, *34*, 163.
(12) Gorman, D.; Drewry, A.; Huang, Y. L.; Sames, C. *Toxicology* **2003**, *187*, 25.
(13) (a) Meyer, O. In *Microbial Gas Metabolism, Mechanistic, Metabolic, and Biotechnological Aspects*; Poole, R. K., Dow, C. S., Eds.; Academic Press: London, 1985. (b) Crutzen, P. J.; Gidel, L. T. *J. Geophys. Res.* **1983**, *88*, 6641.
(14) Motterlini, R.; Otterbein, L. E. *Nat. Rev. Drug Discovery* **2010**, *9*, 728.
(15) Otterbein, L. E.; Soares, M. P.; Yamashita, K.; Bach, F. H. *Trends Immunol.* **2003**, *24*, 449.
(16) King, G. M.; Weber, C. F. *Nat. Rev. Microbiol.* **2007**, *5*, 107.
(17) (a) Daniel, S. L.; Hsu, T.; Dean, S. I.; Drake, H. L. *J. Bacteriol.* **1990**, *172*, 4464. (b) Kerby, R.; Zeikus, J. G. *Curr. Microbiol.* **1983**, *8*, 27.
(18) Uffen, R. L. *J. Bacteriol.* **1983**, *155*, 956.
(19) Svetlichny, V. A.; Sokolova, T. G.; Gerhardt, M.; Ringpfeil, M.; Kostrikina, N. A.; Zavarzin, G. A. *Syst. Appl. Microbiol.* **1991**, *14*, 254.
(20) Meyer, O.; Schlegel, H. G. *Annu. Rev. Microbiol.* **1983**, *37*, 277.
(21) Haldane, J. B. S. *Rationalist Annu.* **1929**, *3*, 3.
(22) Leduc, S. *The Mechanism of Life.*; Rebman: London, UK, 1911.
(23) Martin, W.; Russell, M. J. *Philos. Trans. R. Soc. London, Ser. B* **2007**, *362*, 1887.
(24) Lilley, M. D.; de Angelis, M. A.; Gordon, L. I. *Nature* **1982**, *300*, 48.
(25) Oelgeschlager, E.; Rother, M. *Arch. Microbiol.* **2008**, *190*, 257.
(26) Russell, M. J.; Martin, W. *Trends Biochem. Sci.* **2004**, *29*, 358.
(27) Jaffe, L. S. *Ann. N.Y. Acad. Sci.* **1970**, *174*, 76.
(28) Bartholomew, G. W.; Alexander, M. *Appl. Environ. Microbiol.* **1979**, *37*, 932.
(29) Svetlitchnyi, V.; Peschel, C.; Acker, G.; Meyer, O. *J. Bacteriol.* **2001**, *183*, 5134.
(30) Ragsdale, S. W. *CRC Crit. Rev. Biochem. Mol. Biol.* **2004**, *39*, 165.
(31) (a) Ford, P. A.; Rokicki, A. *Adv. Organometal. Chem.* **1988**, *28*, 139. (b) Kiss, G. *Chem. Rev.* **2001**, *101*, 3435.
(32) Meyer, O.; Rhode, M. In *Microbial Growth on C1 Compounds*; Crawford, R. L., Hanson, R. S., Eds.; American Society for Microbiology: Washington, DC, 1984.
(33) (a) Meyer, O.; Jacobitz, S.; Kruger, B. *FEMS Microbiol. Rev.* **1986**, *39*, 161. (b) Lorite, M. J.; Tachil, J.; Sanjuan, J.; Meyer, O.; Bedmar, E. J. *Appl. Environ. Microbiol.* **2000**, *66*, 1871.
(34) Wilcoxen, J.; Zhang, B.; Hille, R. *Biochemistry* **2011**, *50*, 1910.
(35) Bowien, B.; Schlegel, H. *Annu. Rev. Microbiol.* **1981**, *35*, 405.
(36) Dobbek, H.; Gremer, L.; Kiefersauer, R.; Huber, R.; Meyer, O. *Proc. Natl. Acad. Sci. U.S.A.* **2002**, *99*, 15971.
(37) (a) Zhang, B.; Hemann, C. F.; Hille, R. *J. Biol. Chem.* **2010**, *285*, 12571. (b) Meyer, O.; Gremer, L.; Ferner, R.; Ferner, M.; Dobbek, H.; Gnida, M.; MeyerKlaucke, W.; Huber, R. *Biol. Chem.* **2000**, *381*, 865.
(38) Dobbek, H.; Gremer, L.; Meyer, O.; Huber, R. *Proc. Natl. Acad. Sci. U.S.A.* **1999**, *96*, 8884.
(39) (a) Doukov, T. I.; Iverson, T.; Seravalli, J.; Ragsdale, S. W.; Drennan, C. L. *Science* **2002**, *298*, 567. (b) Darnault, C.; Volbeda, A.; Kim, E. J.; Legrand, P.; Vernede, X.; Lindahl, P. A.; Fontecilla-Camps, J. C. *Nat. Struct. Biol.* **2003**, *10*, 271.
(40) Grahame, D. A. *Biochemistry* **1993**, *32*, 10786.
(41) Pierce, E.; Xie, G.; Barabote, R. D.; Saunders, E.; Han, C. S.; Detter, J. C.; Richardson, P.; Brettin, T. S.; Das, A.; Ljungdahl, L. G.; Ragsdale, S. W. *Environ. Microbiol.* **2008**, *10*, 2550.
(42) Thauer, R. K.; Jungermann, K.; Decker, K. *Bacteriol. Rev.* **1977**, *41*, 100.
(43) Frese, K. W., Jr. In *Electrochemical and Electrocatalytic Reactions of Carbon Dioxide*; Sullivan, B. P., Krist, K., Guard, H. E., Eds.; Elsevier: New York, 1993.
(44) Rosen, B. A.; Salehi-Khojin, A.; Thorson, M. R.; Zhu, W.; Whipple, D. T.; Kenis, P. J. A.; Masel, R. I. *Science* **2011**, *334*, 643.
(45) (a) Parkin, A.; Seravalli, J.; Vincent, K. A.; Ragsdale, S. W.; Armstrong, F. A. *J. Am. Chem. Soc.* **2007**, *129*, 10328. (b) Wang, V. C.; Can, M.; Pierce, E.; Ragsdale, S. W.; Armstrong, F. A. *J. Am. Chem. Soc.* **2013**, *135*, 2198.
(46) Ragsdale, S. W. *J. Inorg. Biochem.* **2007**, *101*, 1657.
(47) Ford, P. C. *Acc. Chem. Res.* **1981**, *14*, 31.
(48) Laine, R. M.; Crawford, E. J. *J. Mol. Catal.* **1988**, *44*, 357.
(49) (a) Holleman, A.; Wiberg, N. *Lehrbuch der Anorganischen Chemie*; Walter de Gruyter & Co.: Hawthorne, NY, 2007. (b) Kim, C. H.; Thompson, L. T. *J. Catal.* **2005**, *230*, 66.
(50) King, R. B. *J. Organomet. Chem.* **1999**, *586*, 2.
(51) Lazarus, O.; Woolerton, T.; Parkin, A.; Lukey, M.; Reisner, E.; Seravalli, J.; Pierce, E.; Ragsdale, S.; Sargent, F.; Armstrong, F. *J. Am. Chem. Soc.* **2009**, *131*, 14154.
(52) Menon, S.; Ragsdale, S. W. *Biochemistry* **1996**, *35*, 15814.
(53) Techtmann, S. M.; Colman, A. S.; Robb, F. T. *Environ. Microbiol.* **2009**, *11*, 1027.
(54) Thauer, R. K. *Microbiol.* **1998**, *144*, 2377.
(55) (a) Burgess, B. K.; Lowe, D. J. *Chem. Rev.* **1996**, *96*, 2983. (b) Hoffman, B. M.; Dean, D. R.; Seefeldt, L. C. *Acc. Chem. Res.* **2009**, *42*, 609. (c) Seefeldt, L. C.; Hoffman, B. M.; Dean, D. R. *Annu. Rev. Biochem.* **2009**, *78*, 701.
(56) Rivera-Ortiz, J. M.; Burris, R. H. *J. Bacteriol.* **1975**, *123*, 537.
(57) (a) Hu, Y.; Lee, C. C.; Ribbe, M. W. *Science* **2011**, *333*, 753. (b) Yang, Z.-Y.; Dean, D. R.; Seefeldt, L. C. *J. Biol. Chem.* **2011**, *286*, 19417.
(58) (a) Yan, L.; Dapper, C. H.; George, S. J.; Wang, H.; Mitra, D.; Dong, W.; Newton, W. E.; Cramer, S. P. *Eur. J. Inorg. Chem.* **2011**, *2011*, 2064. (b) Lee, C. C.; Hu, Y.; Ribbe, M. W. *Science* **2010**, *329*, 642.
(59) Olah, G. A.; Goeppert, A.; Prakash, G. K. S. *Beyond Oil and Gas: The Methanol Economy*; Wiley-VCH: Weinheim, 2006.
(60) (a) Ensign, S. A.; Ludden, P. W. *J. Biol. Chem.* **1991**, *266*, 18395. (b) Seravalli, J.; Kumar, M.; Lu, W. P.; Ragsdale, S. W. *Biochemistry* **1995**, *34*, 7879.
(61) Kumar, M.; Lu, W.-P.; Liu, L.; Ragsdale, S. W. *J. Am. Chem. Soc.* **1993**, *115*, 11646.

(62) (a) Heo, J.; Staples, C. R.; Ludden, P. W. *Biochemistry* **2001**, *40*, 7604. (b) Kumar, M.; Lu, W. P.; Ragsdale, S. W. *Biochemistry* **1994**, *33*, 9769.
(63) Maynard, E. L.; Lindahl, P. A. *J. Am. Chem. Soc.* **1999**, *121*, 9221.
(64) Shin, W.; Lee, S.; Shin, J.; Lee, S.; Kim, Y. *J. Am. Chem. Soc.* **2003**, *125*, 14688.
(65) Menon, S.; Ragsdale, S. W. *Biochemistry* **1996**, *35*, 12119.
(66) Heo, J.; Skjeldal, L.; Staples, C. R.; Ludden, P. W. *J. Biol. Inorg. Chem.* **2002**, *7*, 810.
(67) Lu, W. P.; Ragsdale, S. W. *J. Biol. Chem.* **1991**, *266*, 3554.
(68) Huang, S. Q.; Lindahl, P. A.; Wang, C. Y.; Bennett, G. N.; Rudolph, F. B.; Hughes, J. B. *Appl. Environ. Microbiol.* **2000**, *66*, 1474.
(69) Kumar, M.; Ragsdale, S. W. *J. Am. Chem. Soc.* **1995**, *117*, 11604.
(70) Heo, J.; Wolfe, M. T.; Staples, C. R.; Ludden, P. W. *J. Bacteriol.* **2002**, *184*, 5894.
(71) (a) Drennan, C. L.; Heo, J.; Sintchak, M. D.; Schreiter, E.; Ludden, P. W. *Proc. Natl. Acad. Sci. U.S.A.* **2001**, *98*, 11973. (b) Dobbek, H.; Svetlitchnyi, V.; Gremer, L.; Huber, R.; Meyer, O. *Science* **2001**, *293*, 1281. (c) Dobbek, H.; Svetlitchnyi, V.; Liss, J.; Meyer, O. *J. Am. Chem. Soc.* **2004**, *126*, 5382. (d) Jeoung, J.-H.; Dobbek, H. *Science* **2007**, *318*, 1461. (e) Doukov, T. I.; Blasiak, L. C.; Seravalli, J.; Ragsdale, S. W.; Drennan, C. L. *Biochemistry* **2008**, *47*, 3474. (f) Kung, Y.; Doukov, T. I.; Seravalli, J.; Ragsdale, S. W.; Drennan, C. L. *Biochemistry* **2009**, 7432. (g) Jeoung, J. H.; Dobbek, H. *J. Am. Chem. Soc.* **2009**, *131*, 9922. (h) Jeoung, J. H.; Dobbek, H. *J. Biol. Inorg. Chem.* **2012**, *17*, 167. (i) Gong, W.; Hao, B.; Wei, Z.; Ferguson, D. J., Jr.; Tallant, T.; Krzycki, J. A.; Chan, M. K. *Proc. Natl. Acad. Sci. U. S. A.* **2008**, *105*, 9558.
(72) Craft, J. L.; Ludden, P. W.; Brunold, T. C. *Biochemistry* **2002**, *41*, 1681.
(73) Heo, J.; Halbleib, C. M.; Ludden, P. W. *Proc. Natl. Acad. Sci. U. S. A.* **2001**, *98*, 7690.
(74) Hu, Z. G.; Spangler, N. J.; Anderson, M. E.; Xia, J. Q.; Ludden, P. W.; Lindahl, P. A.; Münck, E. *J. Am. Chem. Soc.* **1996**, *118*, 830.
(75) Anderson, M. E.; Lindahl, P. A. *Biochemistry* **1996**, *35*, 8371.
(76) Russell, W. K.; Lindahl, P. A. *Biochemistry* **1998**, *37*, 10016.
(77) Heo, J.; Staples, C. R.; Telser, J.; Ludden, P. W. *J. Am. Chem. Soc.* **1999**, *121*, 11045.
(78) Spangler, N. J.; Lindahl, P. A.; Bandarian, V.; Ludden, P. W. *J. Biol. Chem.* **1996**, *271*, 7973.
(79) (a) Lindahl, P. A.; Ragsdale, S. W.; Munck, E. *J. Biol. Chem.* **1990**, *265*, 3880. (b) Lindahl, P. A.; Münck, E.; Ragsdale, S. W. *J. Biol. Chem.* **1990**, *265*, 3873.
(80) Ralston, C. Y.; Wang, H. X.; Ragsdale, S. W.; Kumar, M.; Spangler, N. J.; Ludden, P. W.; Gu, W.; Jones, R. M.; Patil, D. S.; Cramer, S. P. *J. Am. Chem. Soc.* **2000**, *122*, 10553.
(81) Gu, W.; Seravalli, J.; Ragsdale, S. W.; Cramer, S. P. *Biochemistry* **2004**, *43*, 9029.
(82) Ragsdale, S. W.; Clark, J. E.; Ljungdahl, L. G.; Lundie, L. L.; Drake, H. L. *J. Biol. Chem.* **1983**, *258*, 2364.
(83) Anderson, M. E.; Lindahl, P. A. *Biochemistry* **1994**, *33*, 8702.
(84) Seravalli, J.; Kumar, M.; Lu, W. P.; Ragsdale, S. W. *Biochemistry* **1997**, *36*, 11241.
(85) (a) Chen, J.; Huang, S.; Seravalli, J.; Gutzman, H., Jr.; Swartz, D. J.; Ragsdale, S. W.; Bagley, K. A. *Biochemistry* **2003**, *42*, 14822. (b) Lindahl, P. A.; Ragsdale, S. W.; Münck, E. *J. Biol. Chem.* **1990**, *265*, 3880. (c) DeRose, V. J.; Telser, J.; Anderson, M. E.; Lindahl, P. A.; Hoffman, B. M. *J. Am. Chem. Soc.* **1998**, *120*, 8767.
(86) Jeoung, J. H.; Dobbek, H. *Science* **2007**, *318*, 1461.
(87) Ermler, U. *Dalton Trans.* **2005**, 3451.
(88) Lee, K. H.; Park, J. H.; Kim, T. Y.; Kim, H. U.; Lee, S. Y. *Mol. Syst. Biol.* **2007**, *3*, 149.
(89) Henry, C. S.; DeJongh, M.; Best, A. A.; Frybarger, P. M.; Linsay, B.; Stevens, R. L. *Nat. Biotechnol.* **2010**, *28*, 977.
(90) Kumar, M.; Lu, W.-P.; Smith, A.; Ragsdale, S. W.; McCracken, J. *J. Am. Chem. Soc.* **1995**, *117*, 2939.
(91) Krzycki, J. A.; Mortenson, L. E.; Prince, R. C. *J. Biol. Chem.* **1989**, *264*, 7217.
(92) Jetten, M. S.; Hagen, W. R.; Pierik, A. J.; Stams, A. J.; Zehnder, A. J. *Eur. J. Biochem.* **1991**, *195*, 385.
(93) Lu, W.-P.; Jablonski, P. E.; Rasche, M.; Ferry, J. G.; Ragsdale, S. W. *J. Biol. Chem.* **1994**, *269*, 9736.
(94) Seravalli, J.; Ragsdale, S. W. *Biochemistry* **2008**, *47*, 6770.
(95) Ensign, S. A. *Biochemistry* **1995**, *34*, 5372.
(96) Bhatnagar, L.; Krzycki, J. A.; Zeikus, J. G. *FEMS Microbiol. Lett.* **1987**, *41*, 337.
(97) Volbeda, A.; Fontecilla-Camps, J. C. *Dalton Trans.* **2005**, 3443.
(98) Wuebbles, D. J.; Hayhoe, K. In *Non-CO_2 Greenhouse Gases: Scientific Understanding, Control and Implementation*; van Ham, J., Baede, A. P. M., Meyer, L. A., Ybema, R., Eds.; Kluwer Academic Publishers: Dordrecht, Netherlands, 2000.
(99) Kerby, R. L.; Ludden, P. W.; Roberts, G. P. *J. Bacteriol.* **1997**, *179*, 2259.
(100) Jeon, W. B.; Cheng, J.; Ludden, P. W. *J. Biol. Chem.* **2001**, *276*, 38602.
(101) Ensign, S. A.; Campbell, M. J.; Ludden, P. W. *Biochemistry* **1990**, *29*, 2162.
(102) Loke, H. K.; Lindahl, P. A. *J. Inorg. Biochem.* **2003**, *93*, 33.
(103) Watt, R. K.; Ludden, P. W. *J. Biol. Chem.* **1998**, *273*, 10019.
(104) Ha, S. W.; Korbas, M.; Klepsch, M.; Meyer-Klaucke, W.; Meyer, O.; Svetlitchnyi, V. *J. Biol. Chem.* **2007**, *282*, 10639.
(105) (a) Feist, A. M.; Henry, C. S.; Reed, J. L.; Krummenacker, M.; Joyce, A. R.; Karp, P. D.; Broadbelt, L. J.; Hatzimanikatis, V.; Palsson, B. O. *Mol. Syst. Biol.* **2007**, *3*, 18. (b) Mahadevan, R.; Bond, D. R.; Butler, J. E.; Esteve-Nunez, A.; Coppi, M. V.; Palsson, B. O.; Schilling, C. H.; Lovley, D. R. *Appl. Environ. Microbiol.* **2006**, *72*, 1558.
(106) (a) Ensign, S. A.; Hyman, M. R.; Ludden, P. W. *Biochemistry* **1989**, *28*, 4973. (b) Diekert, G. B.; Thauer, R. K. *J. Bacteriol.* **1978**, *136*, 597.
(107) Drake, H. L.; Hu, S.-I.; Wood, H. G. *J. Biol. Chem.* **1980**, *255*, 7174.
(108) Lindahl, P. A. *Angew. Chem., Int. Ed.* **2008**, *47*, 4054.
(109) Ensign, S. A.; Bonam, D.; Ludden, P. W. *Biochemistry* **1989**, *28*, 4968.
(110) Svetlitchnyi, V.; Dobbek, H.; Meyer-Klaucke, W.; Meins, T.; Thiele, B.; Romer, P.; Huber, R.; Meyer, O. *Proc. Natl. Acad. Sci. U.S.A.* **2004**, *101*, 446.
(111) Price, N. D.; Papin, J. A.; Palsson, B. O. *Genome Res.* **2002**, *12*, 760.
(112) Kim, E. J.; Feng, J.; Bramlett, M. R.; Lindahl, P. A. *Biochemistry* **2004**, *43*, 5728.
(113) Fontecilla-Camps, J. C.; Volbeda, A.; Cavazza, C.; Nicolet, Y. *Chem. Rev.* **2007**, *107*, 4273.
(114) Amara, P.; Mouesca, J. M.; Volbeda, A.; Fontecilla-Camps, J. C. *Inorg. Chem.* **2011**, *50*, 1868.
(115) Lindahl, P. A. *J. Biol. Inorg. Chem.* **2004**, *9*, 516.
(116) Page, C. C.; Moser, C. C.; Chen, X. X.; Dutton, P. L. *Nature* **1999**, *402*, 47.
(117) Anderson, M. E.; DeRose, V. J.; Hoffman, B. M.; Lindahl, P. A. *J. Inorg. Biochem.* **1993**, *51*, Abstract B149.
(118) Wang, P. H.; Bruschi, M.; De Gioia, L.; Blumberger, J. *J. Am. Chem. Soc.* **2013**, *135*, 9493.
(119) Tan, G. O.; Ensign, S. A.; Ciurli, S.; Scott, M. J.; Hedman, B.; Holm, R. H.; Ludden, P. W.; Korszun, Z. R.; Stephens, P. J.; Hodgson, K. O. *Proc. Natl. Acad. Sci. U. S. A.* **1992**, *89*, 4427.
(120) Ciurli, S.; Ross, P. K.; Scott, M. J.; Yu, S.-B.; Holm, R. H. *J. Am. Chem. Soc.* **1992**, *114*, 5415.
(121) Sun, J.; Sayyar, B.; Butler, J. E.; Pharkya, P.; Fahland, T. R.; Famili, I.; Schilling, C. H.; Lovley, D. R.; Mahadevan, R. *BMC Syst. Biol.* **2009**, *3*, 15.
(122) Smith, D. M. A.; Danyal, K.; Seefeldt, L. C. *Biochemistry* **2013**, in press.
(123) Smith, D. M. A.; Rosso, K. M. *Biophys. J.* **2013**, in press.
(124) (a) Panda, R.; Zhang, Y.; McLauchlan, C. C.; Venkateswara Rao, P.; Tiago de Oliveira, F. A.; Munck, E.; Holm, R. H. *J. Am. Chem. Soc.* **2004**, *126*, 6448. (b) Sun, J.; Tessier, C.; Holm, R. H. *Inorg. Chem.* **2007**, *46*, 2691.

(125) Bell, A. T. *DOE Rep.* **2008**, http://www.sc.doe.gov/bes/reports/files/CAT_rpt.pdf.
(126) Dubois, M. R.; Dubois, D. L. *Acc. Chem. Res.* **2009**, *42*, 1974.
(127) Fisher, B.; Eisenberg, R. *J. Am. Chem. Soc.* **1980**, *102*, 7361.
(128) Beley, M.; Collin, J. P.; Ruppert, R.; Sauvage, J. P. *J. Am. Chem. Soc.* **1986**, *108*, 7461.
(129) (a) Fujita, E.; Creutz, C.; Sutin, N.; Szalda, D. J. *J. Am. Chem. Soc.* **1991**, *113*, 343. (b) Schmidt, M. H.; Miskeley, G. M.; Lewis, N. S. *J. Am. Chem. Soc.* **1990**, *112*, 3240.
(130) Fujita, E.; Creutz, C.; Sutin, N.; Brunschwig, B. S. *Inorg. Chem.* **1993**, *32*, 2657.
(131) Johnson, E. F.; Mukhopadhyay, B. *Appl. Environ. Microbiol.* **2008**, *74*, 3591.
(132) Dodsworth, J. A.; Leigh, J. A. *Proc. Natl. Acad. Sci. U. S. A.* **2006**, *103*, 9779.
(133) Haydock, A. K.; Porat, I.; Whitman, W. B.; Leigh, J. A. *FEMS Microbiol. Lett.* **2004**, *238*, 85.
(134) Zomorrodi, A. R.; Suthers, P. F.; Ranganathan, S.; Maranas, C. D. *Metab. Eng.* **2012**, *14*, 672.
(135) Bhugun, I.; Lexa, D.; Savéant, J.-M. *J. Am. Chem. Soc.* **1996**, *118*, 1769.
(136) Milne, C. B.; Kim, P. J.; Eddy, J. A.; Price, N. D. *Biotechnol. J.* **2009**, *4*, 1653.
(137) Thiele, I.; Palsson, B. O. *Nat. Protoc.* **2010**, *5*, 93.
(138) Gibson, D. H. *Chem. Rev.* **1996**, *96*, 2063.
(139) Stolyar, S.; Van Dien, S.; Hillesland, K. L.; Pinel, N.; Lie, T. J.; Leigh, J. A.; Stahl, D. A. *Mol. Syst. Biol.* **2007**, *3*, 92.
(140) Huang, D. G.; Holm, R. H. *J. Am. Chem. Soc.* **2010**, *132*, 4693.
(141) Vincent, K. A.; Parkin, A.; Armstrong, F. A. *Chem. Rev.* **2007**, *107*, 4366.
(142) Armstrong, F. A.; Hirst, J. *Proc. Natl. Acad. Sci. U. S. A.* **2011**, *108*, 14049.
(143) Hexter, S. V.; Grey, F.; Happe, T.; Climent, V.; Armstrong, F. A. *Proc. Natl. Acad. Sci. U.S.A.* **2012**, *109*, 11516.
(144) Wang, V. C.-C.; Ragsdale, S. W.; Armstrong, F. A. *ChemBioChem* **2013**, *14*, 1845.
(145) Woolerton, T. W.; Sheard, S.; Chaudhary, Y. S.; Armstrong, F. A. *Energy Environ. Sci.* **2012**, *5*, 7470.
(146) Nazeeruddin, M. K.; Kay, A.; Rodicio, I.; Humphry-Baker, R.; Mueller, E.; Liska, P.; Vlachopoulos, N.; Grätzel, M. *J. Am. Chem. Soc.* **1993**, *115*, 6382.
(147) (a) Woolerton, T. W.; Sheard, S.; Pierce, E.; Ragsdale, S. W.; Armstrong, F. A. *Energy Environ. Sci.* **2011**, *4*, 2393. (b) Woolerton, T. W.; Sheard, S.; Reisner, E.; Pierce, E.; Ragsdale, S. W.; Armstrong, F. A. *J. Am. Chem. Soc.* **2010**, *132*, 2132.
(148) Chaudhary, Y. S.; Woolerton, T. W.; Allen, C. S.; Warner, J. H.; Pierce, E.; Ragsdale, S. W.; Armstrong, F. A. *Chem. Commun.* **2012**, *48*, 58.
(149) *Applied Homogeneous Catalysis with Organometallic Compounds*, 2nd ed.; Cornils, B., Herrmann, W. A., Eds.; Wiley-VCH: Weinheim, 2002.
(150) Ragsdale, S. W.; Kumar, M. *Chem. Rev.* **1996**, *96*, 2515.
(151) van Leeuwen, P. W. N. M. *Homogeneous Catalysis: Understanding the Art*; Kluwer: Dordrecht, 2004.
(152) Ragsdale, S. W.; Wood, H. G. *J. Biol. Chem.* **1985**, *260*, 3970.
(153) (a) Grahame, D. A. *J. Biol. Chem.* **1991**, *266*, 22227. (b) Terlesky, K. C.; Nelson, M. J. K.; Ferry, J. G. *J. Bacteriol.* **1986**, *168*, 1053.
(154) Seravalli, J.; Gu, W.; Tam, A.; Strauss, E.; Begley, T. P.; Cramer, S. P.; Ragsdale, S. W. *Proc. Natl. Acad. Sci. U. S. A.* **2003**, *100*, 3689.
(155) Ragsdale, S. W.; Wood, H. G.; Antholine, W. E. *Proc. Natl. Acad. Sci. U. S. A.* **1985**, *82*, 6811.
(156) Shin, W.; Anderson, M. E.; Lindahl, P. A. *J. Am. Chem. Soc.* **1993**, *115*, 5522.
(157) Shin, W.; Lindahl, P. A. *Biochemistry* **1992**, *31*, 12870.
(158) Seravalli, J.; Gu, W. W.; Tam, A.; Strauss, E.; Begley, T. P.; Cramer, S. P.; Ragsdale, S. W. *Proc. Natl. Acad. Sci. U. S. A.* **2003**, *100*, 3689.
(159) Seravalli, J.; Xiao, Y.; Gu, W.; Cramer, S. P.; Antholine, W. E.; Krymov, V.; Gerfen, G. J.; Ragsdale, S. W. *Biochemistry* **2004**, *43*, 3944.
(160) Bramlett, M. R.; Tan, X.; Lindahl, P. A. *J. Am. Chem. Soc.* **2003**, *125*, 9316.
(161) Seravalli, J.; Ragsdale, S. W. *Biochemistry* **2000**, *39*, 1274.
(162) Maynard, E. L.; Lindahl, P. A. *Biochemistry* **2001**, *40*, 13262.
(163) Bender, G.; Stich, T. A.; Yan, L.; Britt, R. D.; Cramer, S. P.; Ragsdale, S. W. *Biochemistry* **2010**, *49*, 7516.
(164) (a) Tan, X.; Volbeda, A.; Fontecilla-Camps, J. C.; Lindahl, P. A. *J. Biol. Inorg. Chem.* **2006**, *11*, 371. (b) Tan, X.; Loke, H. K.; Fitch, S.; Lindahl, P. A. *J. Am. Chem. Soc.* **2005**, *127*, 5833. (c) Tan, X.; Lindahl, P. A. *J. Biol. Inorg. Chem.* **2008**, *13*, 771.
(165) Shanmugasundaram, T.; Wood, H. G. *J. Biol. Chem.* **1992**, *267*, 897.
(166) (a) Shanmugasundaram, T.; Kumar, G. K.; Wood, H. G. *Biochemistry* **1988**, *27*, 6499. (b) Ragsdale, S. W.; Wood, H. G. *J. Biol. Chem.* **1985**, *260*, 3970.
(167) Volbeda, A.; Darnault, C.; Tan, X.; Lindahl, P. A.; Fontecilla-Camps, J. C. *Biochemistry* **2009**, *48*, 7916.
(168) Funk, T.; Gu, W.; Friedrich, S.; Wang, H.; Gencic, S.; Grahame, D. A.; Cramer, S. P. *J. Am. Chem. Soc.* **2004**, *126*, 88.
(169) Park, J. H.; Lee, K. H.; Kim, T. Y.; Lee, S. Y. *Proc. Natl. Acad. Sci. U. S. A.* **2007**, *104*, 7797.
(170) Seravalli, J.; Ragsdale, S. W. *J. Biol. Chem.* **2008**, *283*, 8384.
(171) Ragsdale, S. W. *Chem. Rev.* **2006**, *106*, 3317.
(172) Forster, D. J. *J. Am. Chem. Soc.* **1976**, *98*, 846.
(173) Forster, D. J. *Adv. Organomet. Chem.* **1979**, *17*, 255.
(174) Ramer, S. E.; Raybuck, S. A.; Orme-Johnson, W. H.; Walsh, C. T. *Biochemistry* **1989**, *28*, 4675.
(175) Lu, W. P.; Harder, S. R.; Ragsdale, S. W. *J. Biol. Chem.* **1990**, *265*, 3124.
(176) Tan, X. S.; Sewell, C.; Lindahl, P. A. *J. Am. Chem. Soc.* **2002**, *124*, 6277.
(177) Tan, X.; Sewell, C.; Yang, Q.; Lindahl, P. A. *J. Am. Chem. Soc.* **2003**, *125*, 318.
(178) Seravalli, J.; Kumar, M.; Ragsdale, S. W. *Biochemistry* **2002**, *41*, 1807.
(179) Bramlett, M. R.; Stubna, A.; Tan, X. S.; Surovtsev, I. V.; Munck, E.; Lindahl, P. A. *Biochemistry* **2006**, *45*, 8674.
(180) Tan, X.; Martinho, M.; Stubna, A.; Lindahl, P. A.; Munck, E. *J. Am. Chem. Soc.* **2008**, *130*, 6712.
(181) Fan, C. L.; Gorst, C. M.; Ragsdale, S. W.; Hoffman, B. M. *Biochemistry* **1991**, *30*, 431.
(182) Xia, J. Q.; Hu, Z. G.; Popescu, C. V.; Lindahl, P. A.; Munck, E. *J. Am. Chem. Soc.* **1997**, *119*, 8301.
(183) (a) Kumar, M.; Ragsdale, S. W. *J. Am. Chem. Soc.* **1992**, *114*, 8713. (b) George, S. J.; Seravalli, J.; Ragsdale, S. W. *J. Am. Chem. Soc.* **2005**, *127*, 13500.
(184) Peters, J. W.; Lanzilotta, W. N.; Lemon, B. J.; Seefeldt, L. C. *Science* **1998**, *282*, 1853.
(185) Nicolet, Y.; Lemon, B. J.; Fontecilla-Camps, J. C.; Peters, J. W. *Trends Biochem. Sci.* **2000**, *25*, 138.
(186) (a) Schenker, R. P.; Brunold, T. C. *J. Am. Chem. Soc.* **2003**, *125*, 13962. (b) Brunold, T. C. *J. Biol. Inorg. Chem.* **2004**, *9*, 533.
(187) Ragsdale, S. W.; Ljungdahl, L. G.; DerVartanian, D. V. *Biochem. Biophys. Res. Commun.* **1983**, *115*, 658.
(188) Bender, G.; Ragsdale, S. W. *Biochemistry* **2011**, *50*, 276.
(189) Gorst, C. M.; Ragsdale, S. W. *J. Biol. Chem.* **1991**, *266*, 20687.
(190) Segre, D.; Vitkup, D.; Church, G. M. *Proc. Natl. Acad. Sci. U. S. A.* **2002**, *99*, 15112.
(191) Barondeau, D. P.; Lindahl, P. A. *J. Am. Chem. Soc.* **1997**, *119*, 3959.
(192) Ram, M. S.; Riordan, C. G. *J. Am. Chem. Soc.* **1995**, *117*, 2365.
(193) Ram, M. S.; Riordan, C. G.; Yap, G. P. A.; Liable-Sands, L.; Rheingold, A. L.; Marchaj, A.; Norton, J. R. *J. Am. Chem. Soc.* **1997**, *119*, 1648.
(194) Martin, B. D.; Finke, R. G. *J. Am. Chem. Soc.* **1990**, *112*, 2419.
(195) Gencic, S.; Grahame, D. A. *Biochemistry* **2008**, *47*, 5544.

(196) Harrop, T. C.; Mascharak, P. K. *Coord. Chem. Rev.* **2005**, *249*, 3007.
(197) Linck, R. C.; Spahn, C. W.; Rauchfuss, T. B.; Wilson, S. R. *J. Am. Chem. Soc.* **2003**, *125*, 8700.
(198) (a) Krishnan, R.; Riordan, C. G. *J. Am. Chem. Soc.* **2004**, *126*, 4484. (b) Rao, P. V.; Bhaduri, S.; Jiang, J.; Holm, R. H. *Inorg. Chem.* **2004**, *43*, 5833.
(199) Harrop, T. C.; Olmstead, M. M.; Mascharak, P. K. *J. Am. Chem. Soc.* **2004**, *126*, 14714.
(200) Harrop, T. C.; Olmstead, M. M.; Mascharak, P. K. *Inorg. Chem.* **2006**, *45*, 3424.
(201) Harrop, T. C.; Olmstead, M. M.; Mascharak, P. K. *Chem. Commun.* **2004**, 1744.
(202) (a) Marganian, C. A.; Vazir, H.; Baidya, N.; Olmstead, M. M.; Mascharak, P. K. *J. Am. Chem. Soc.* **1995**, *117*, 1584. (b) Baidya, N.; Olmstead, M.; Whitehead, J. P.; Bagyinka, C.; Maroney, M. J.; Mascharak, P. K. *Inorg. Chem.* **1992**, *31*, 3612.
(203) Matsumoto, T.; Ito, M.; Kotera, M.; Tatsumi, K. *Dalton Trans.* **2010**, *39*, 2995.
(204) Eckert, N. A.; Dougherty, W. G.; Yap, G. P.; Riordan, C. G. *J. Am. Chem. Soc.* **2007**, *129*, 9286.
(205) Dougherty, W. G.; Rangan, K.; O'Hagan, M. J.; Yap, G. P. A.; Riordan, C. G. *J. Am. Chem. Soc.* **2008**, *130*, 13510.
(206) Ariyananda, P. W. G.; Kieber-Emmons, M. T.; Yap, G. P. A.; Riordan, C. G. *Dalton Trans.* **2009**, 4359.
(207) Ito, M.; Kotera, M.; Matsumoto, T.; Tatsumi, K. *Proc. Natl. Acad. Sci. U. S. A.* **2009**, *106*, 11862.
(208) Horn, B.; Limberg, C.; Herwig, C.; Mebs, S. *Angew. Chem., Int. Ed.* **2011**, *50*, 12621.
(209) Sebaihia, M.; Wren, B. W.; Mullany, P.; Fairweather, N. F.; Minton, N.; Stabler, R.; Thomson, N. R.; Roberts, A. P.; Cerdeno-Tarraga, A. M.; Wang, H.; Holden, M. T.; Wright, A.; Churcher, C.; Quail, M. A.; Baker, S.; Bason, N.; Brooks, K.; Chillingworth, T.; Cronin, A.; Davis, P.; Dowd, L.; Fraser, A.; Feltwell, T.; Hance, Z.; Holroyd, S.; Jagels, K.; Moule, S.; Mungall, K.; Price, C.; Rabbinowitsch, E.; Sharp, S.; Simmonds, M.; Stevens, K.; Unwin, L.; Whithead, S.; Dupuy, B.; Dougan, G.; Barrell, B.; Parkhill, J. *Nat. Genet.* **2006**, *38*, 779.

NOTE ADDED AFTER ASAP PUBLICATION

This was published on 2/13/2014, with errors in Figure 2 and Scheme 2. These were fixed in the version published on 2/20/2014.